Acta Pharmaceutica Sinica B 2024;14(9):3964–3982

Chinese Pharmaceutical Association
Institute of Materia Medica, Chinese Academy of Medical Sciences

Acta Pharmaceutica Sinica B

www.elsevier.com/locate/apsb
www.sciencedirect.com

ORIGINAL ARTICLE

Aloe emodin promotes mucosal healing by modifying the differentiation fate of enteroendocrine cells *via* regulating cellular free fatty acid sensitivity

Weilian Bao [a,b,†], Jiaren Lyu [a,b,†], Guize Feng [a,†], Linfeng Guo [b], Dian Zhao [b], Keyuan You [a], Yang Liu [b], Haidong Li [a], Peng Du [c,d], Daofeng Chen [b,*], Xiaoyan Shen [a,*]

[a]*Department of Pharmacology & the Key Laboratory of Smart Drug Delivery Ministry of Education, School of Pharmacy, Fudan University, Shanghai 201210, China*
[b]*Department of Natural Medicine, School of Pharmacy, Fudan University, Shanghai 201210, China*
[c]*Department of Colorectal and Anal Surgery, Xinhua Hospital, Shanghai Jiao Tong University School of Medicine, Shanghai 200092, China*
[d]*Shanghai Colorectal Cancer Research Center, Shanghai 200092, China*

Received 25 December 2023; received in revised form 8 March 2024; accepted 12 April 2024

KEY WORDS

LRCs;
ISCs;
EECs;
IBD;
SOX9;
Aloe emodin;
FFAR1;
FOXO1

Abstract The proper differentiation and reorganization of the intestinal epithelial cell population is critical to mucosal regeneration post injury. Label retaining cells (LRCs) expressing SRY-box transcription factor 9 (SOX9) promote epithelial repair by replenishing $LGR5^+$ intestinal stem cells (ISCs). While, LRCs are also considered precursor cells for enteroendocrine cells (EECs) which exacerbate mucosal damage in inflammatory bowel disease (IBD). The factors that determine LRC-EEC differentiation and the effect of intervening in LRC-EEC differentiation on IBD remain unclear. In this study, we investigated the effects of a natural anthraquinone called aloe emodin (derived from the Chinese herb rhubarb) on mucosal healing in IBD models. Our findings demonstrated that aloe emodin effectively interfered with the differentiation to EECs and preserved a higher number of $SOX9^+$ LRCs, thereby promoting mucosal healing. Furthermore, we discovered that aloe emodin acted as an antagonist of free fatty acid receptors (FFAR1), suppressing the FFAR1-mediated G$\beta\gamma$/serine/threonine-protein kinase (AKT) pathway and promoting the translocation of forkhead box protein O1 (FOXO1) into the nucleus,

*Corresponding authors.
E-mail addresses: shxiaoy@fudan.edu.cn (Xiaoyan Shen), dfchen@shmu.edu.cn (Daofeng Chen).
[†]These authors made equal contributions to this work.
Peer review under the responsibility of Chinese Pharmaceutical Association and Institute of Materia Medica, Chinese Academy of Medical Sciences.

https://doi.org/10.1016/j.apsb.2024.05.027

ultimately resulting in the intervention of differentiation fate. These findings reveal the effect of free fatty acid accessibility on EEC differentiation and introduce a strategy for promoting mucosal healing in IBD by regulating the FFAR1/AKT/FOXO1 signaling pathway.

1. Introduction

Mucosal healing is key prognostic indicator for long-term remission and reduced surgical risk in inflammatory bowel disease (IBD) patients[1]. An unhealed mucosa means that damaged epithelium causes translocation of intestinal luminal contents, including commensal bacteria and pathogenic microorganisms to the lamina propria, hence causing persistent inflammation[2]. Under normal conditions, $LGR5^+$ crypt basal columnar cells (CBCs)/activated intestinal stem cells (aISCs) gradually differentiate upward into different types of intestinal epithelial cells for epithelial integrity[3]. However, the self-renew function of CBCs is impaired in Crohn's disease (CD) patients and mice models, leading to the unhealed mucosa and relapsing inflammation[4-7]. SRY-box transcription factor 9 (SOX9) + label-retaining cells (LRCs)/reserve ISCs (rISCs) are activated from the quiescence state and transformed into CBCs post radiation injury[8-10]. The role of LRCs in IBD remains unclear, but its progeny, enteroendocrine cells (EECs), increase abnormally in patients with ulcerative colitis (UC) and CD[3,11,12]. Inhibition of 5-hydroxytryptamine (5-HT) and chromogranin A (CHGA) produced by EEC alleviates colitis in mice[13,14]. Hence, interrupting the LRC-EEC differentiation axis to retain more LRCs theoretically promotes mucosal healing in IBD.

Rhubarb is an umbrella name for various perennial plants of the genus *Rheum* L. from the *Polygonaceae* family, which has been used as a laxative in China since the 3rd millennium B.C. The excellent laxative effect of rhubarb implies that it might contain compounds that regulate the intestinal physiological activity; nonetheless, convincing systematic studies are lacking. The major chemical constituents of rhubarb include anthraquinones, anthrone, zhienes, etc[15]. In the present study, we screened the major components in rhubarb using dextran sulfate sodium salt (DSS)-induced IBD models and found that aloe emodin significantly alleviates the colitis. Aloe emodin (1,8-dihydroxy-3-hydroxymethylanthraquinone), one of the natural anthraquinone derivatives, exerts antitumor, antiviral, anti-inflammatory, antibacterial, and hepatoprotective pharmacological effects without a convincing direct target[16]. Our findings demonstrated that aloe emodin directly antagonizes the activation of free fatty acid receptor 1 (FFAR1), and suppresses serine/threonine-protein kinase (AKT)-mediated phosphorylation and nuclear export of forkhead box protein O1 (FOXO1). Then, relatively increased nuclear import of FOXO1 leads to high SOX9 expression, which inhibits differentiation of LRC to EEC and facilitated epithelium reconstruction.

2. Materials and methods

2.1. Materials

Details (including RRID or CAS numbers) of all materials used in this study (including antibodies, reagents, animals, commercial assays, cells, primers, software and deposited data, etc.) are placed in Supporting Information Tables S1−S3.

2.2. Human samples

Sections for immunofluorescence staining were obtained from excised samples of colon lesions from CD patients. The CD patients were enrolled and followed up from July 2010 to July 2020 at the Department of Colorectal Surgery, Xinhua Hospital, Shanghai Jiao Tong University School of Medicine. The CD was diagnosed using clinical, endoscopic, and histologic criteria. The study complied with the Helsinki Declaration, and the study protocol was approved by the Institutional Ethics Committee of Xinhua Hospital affiliated to Shanghai Jiaotong University School of Medicine. All the patients included in the study signed the informed consent.

2.3. Cell culture

Human Caco-2 cells and human embryonic kidney (HEK) 293T cells purchased from American Type Culture Collection (ATCC) were cultured in high glucose Dulbecco's modified Eagle's medium (DMEM) supplemented with FBS (fetal bovine serum, 20% for Caco-2 cells, 10% for HEK 293T cells) at 37 °C under 5% (*v*/*v*) CO_2 atmosphere.

2.4. Colon crypt isolation and three-dimensional culture

Colon organoid culture was modified based on the previous protocol[17]. Briefly, after euthanizing the mice, colons were longitudinally opened and washed with phosphate-buffered saline (PBS). To dissociate the crypts, tissues were incubated at 37 °C in ethylenediaminetetraacetic acid (EDTA) buffer (2 mmol/L EDTA, 43.4 mmol/L sucrose, 54.9 mmol/L D-sorbitol, 0.5 mmol/L D,L-dithiothreitol) for 30 min. The isolated crypts were incubated with TrypLE Express (Gibco) at 37 °C for 1 h to break them up into individual cells. Colon epithelial cells were suspended in 50% matrigel with 50% advanced DMEM/F12 medium. After 20-min incubation to polymerize matrigel, WENR medium (epidermal growth factor (EGF), Noggin and Rspondin-1 containing medium plus 10% Wnt3a conditioned medium) was added.

2.5. Quality control of aloe emodin

Aloe emodin was purchased from Shanghai Standard Technology Co., Ltd. (batch No. 14346). Quality control of aloe emodin was performed using the ultra-high performance liquid chromatography (UPLC) system equipped with an AB triple time-of-flight (TOF) 5600 plus System (Framingham, MA, USA) along with a YMC-Triart C18 column (150 mm × 2.1 mm, 1.9 μm). The

mobile phase was acetonitrile and 0.1% phosphoric acid solution operating at a flow rate of 0.3 mL/min. UV detections were performed at 256 nm for aloe emodin and 288 nm for emodin. Electrospray ionization (ESI) was selected as the ionization source and negative ionization mode was set as the detection mode. The ion spray voltage was 5.50 kV with transfer capillary temperature at 550 °C. The scan mass range was set from *m/z* 50−1500.

2.6. *Immunostaining and immunohistochemistry*

Organoids in the plates were fixed with 4% paraformaldehyde at 4 °C for 45 min. Then, organoids were treated with PBS containing 10% goat serum, 10% dimethyl sulfoxide (DMSO) and 2% Triton-X for 1 h. Caco-2 cells were fixed with 4% paraformaldehyde at 4 °C for 10 min and permeated with 0.1% Triton-X for 10 min and blocked with 10% goat serum for 2 h. Cells or organoids were then incubated with primary antibodies at room temperature for 2 h. After washing three times with PBS, cells or organoids were incubated with appropriate Alexa Fluor-labeled secondary antibodies in the blocking buffer at room temperature for 2 h. The slides were sealed by mounting media containing DAPI and then observed under a laser scanning confocal microscope (Zeiss, Germany)[18]. Co-localization analysis was completed by Image J's JACop plugin.

Tissue samples were fixed in 4% paraformaldehyde and embedded in paraffin. Tissue embedding, sectioning and H&E staining were performed by Servicebio Inc. (Shanghai, China). For immunofluorescence staining, sections were deparaffinized with standard techniques and incubated with primary antibodies overnight at 4 °C, and then incubated with secondary antibodies at room temperature for 30 min. The immunofluorescence staining sections were pictured by an inverted phase contrast fluorescence microscope (Olympus, Tokyo, Japan). The positive cell count was completed by Image J.

2.7. *In vivo experiments*

8-week-old male C57BL/6 mice were grouped using a completely randomized method and induced by 3% DSS for 7 days (except control group). Mice that received DSS were administered with compounds intragastrically once daily throughout the course (for compound screening) or after the onset of symptoms (for pharmacodynamic experiments of aloe emodin).

For 2,4,6-trinitrobenzene sulfonic acid (TNBS) model, we used a standard single-application TNBS model of 8-week-old female BALB/c mice. Briefly, mice were fasted for 24 h before the experiment and after ether anesthesia. A 2.0 mm diameter syringe hose was lubricated with paraffin oil and gently inserted into the anus before slowly injecting 200 μL of 5% TNBS/50% ethanol (1:1) solution (normal control group was instilled with PBS solution); the tail was lifted thereafter. The mice were kept lying flat and naturally awake after 5 min of continuous inversion[19]. The mice that received TNBS were intragastrically administered with compounds once daily after the onset of symptoms.

Mice were weighed and scored for disease activity index (DAI) daily. DAI was assessed terminally by an unbiased observer based on a previously published scoring system[20]. Each mouse was scored from four aspects: rectal bleeding, rectal prolapse, stool consistency and blood, each with a score of 0 to 3. On the indicated day, the mice were sacrificed to obtain colon tissues and blood.

2.8. *In vivo intestinal permeability assay*

The intestinal barrier integrity was assessed using fluorescein isothiocyanate (FITC)-dextran as previously described[21]. In brief, mice were starved for 4 h and then gavaged with 600 mg/kg FITC-dextran followed by 4 h fasting before euthanization. The content of FITC-dextran in serum was measured based on the standard curve by a microplate reader at a 480-nm excitation wavelength and a 525-nm emission wavelength.

2.8.1. *Isolation of colonic epithelial cells*

Colonic epithelial cells were isolated using a protocol as described[22]. Briefly, colon tissues from mice were longitudinally opened and flushed with ice-cold PBS. Tissues were cut into small pieces (1 cm) and vigorously shaken in Hanks' balanced salt solution (HBSS) containing 40 mmol/L EDTA and 1 mmol/L dithiothreitol (DTT) at 37 °C for 20 min and then passed through a 100 μm cell strainer. Epithelial cells in the filtering liquid were collected and centrifuged at 300× *g* at 4 °C for 10 min. In order to further exclude other cells, CD326 (EpCAM) and CD45 selection kit were used to select $EpCAM^{+}CD45^{-}$ epithelial cells for subsequent measurements.

2.9. *DNA pull-down assay*

Potential binding sites for the FOXO1 and SOX9 promoter regions (−2000 to −1) were predicted by the JASPAR website (https://jaspar.genereg.net). PCR primers were designed according to the FOXO1-binding sequences so that the PCR products were ∼500 bp. Then, the PCR products were labeled with biotin using Biotin-11-dUTP and a specific primer. The gel recovery kit was used to isolate a labeled probe from agarose gels. Nuclear and Cytoplasmic Protein Extraction Kit was used to extract nuclear protein, and the protein concentration was measured by bicinchoninic acid assay (BCA). Biotin-labeled probe corresponding to SOX9 promoter (1 μg) was incubated with nuclear protein (70 μg). One hour after incubation, streptavidin-coated beads were added to isolate the DNA−protein complex. The protein was eluted and then run on sodium dodecyl sulfate-polyacrylamide gel electrophoresis (SDS-PAGE).

2.10. *RNA sequencing of colonic epithelial cells from colitis mice*

The mRNA was purified from 1 μg total RNA using oligo (dT) magnetic beads followed by fragmentation carried out using divalent cations at elevated temperatures. Subsequently, first-strand and second-strand cDNAs were synthesized, followed by PCR amplification. PCR products were purified (AMPure XP system) and library quality was assessed on an Agilent Bioanalyzer 4150 system. Finally, sequencing was performed with an Illumina Novaseq 6000/MGISEQ-T7 instrument. Raw reads of fastq format were firstly processed through in-house perl scripts. In this step, the adapter sequence, low quality (low quality, the number of lines with a string quality value less than or equal to 25 accounts for more than 60% of the entire reading), as well as N (N means that the base information cannot be determined) ratio is greater than 5% reads were removed to obtain clean reads that can

be used for subsequent analysis. Then clean reads were separately aligned to the reference genome with orientation mode using HISAT2 software (http://daehwankimlab.github.io/hisat2/) to obtain mapped reads. FeatureCounts (http://subread.sourceforge.net/) was used to count the read numbers mapped to each gene. And then FPKM of each gene was calculated based on the length of the gene and reads count mapped to this gene. RNA-sequencing was performed by Applied Protein Technology (Shanghai, China).

2.11. Chromatin immunoprecipitation (ChIP)-qPCR assay

Caco-2 cells were cross-linked with 1% formaldehyde for 10 min. The ChIP assay was performed by using anti-FOXO1 and the ChIP assay kit (Beyotime, Shanghai, China) according to the manufacturer's instructions. Normal rabbit IgG was also used as a negative control. The bound DNA fragments were subjected to real-time PCR analysis using the specific primers shown in Supporting Information Table S2.

2.12. Construction of knockout cell line or organoid and reintroduction assay

Single guide RNA (sgRNA) targeting the human *FOXO1* sequence was: GGTGGCGCAAACGAGTAGCA, while sgRNA targeting murine *Foxo1* sequence was TGATGAGGTCGGCGTACGAC (designed by www.zlab.bio/guide-design-resources and validated by previous study[23,24]). The sgRNA targeting murine Sox9 sequence was ACCAGCCGAGTCCTCCGACA. Lentivirus (Lenti-CAS9-sgRNA-puro) encoding Cas9 and sgRNA targeting FOXO1 or the control vector was constructed and packed on HEK 293T. Cultured Caco-2 cells were infected with Lentivirus-CAS9-sgRNA-puromycin. After 72 h, puromycin was used to select the FOXO1 CRISPRko cells. For reintroduction of FOXO1, Flag-FOXO1 was constructed on pcDNA3.1 vector. FOXO1 CRISPRko cells were transfected with the Flag-Vector or Flag-FOXO1 using the PolyJet transfection reagent.

Construction of FOXO1 or SOX9 knockout organoids were performed as previous protocol[25]. Mouse colon organoids were resuspended in Tryple Express followed by incubation at 37 °C for 5 min. After centrifugation at 900 × *g*, the pellet was resuspended in 250 μL of virus solution. The mixture was then centrifuged at 600× *g* for 1 h at 32 °C then incubated at 37 °C for 6 h, followed by centrifugation and cooling on ice. Subsequently, 100 μL of Matrigel was added and mixed, and the mixture was seeded into 48-well plates. Transformation medium (WENR medium supplemented with 10 mmol/L nicotinic acid (NAM), 10 μmol/L Y-27632, and 5 μmol/L CHIR99021) was added for culture. After three days, organoids were screened with puromycin-containing transformation medium. When the crypts started to grow, the transformation medium was replaced with WENR medium containing puromycin to support further crypt growth.

2.13. Docking

The 3D sdf file of aloe emodin was downloaded from the PubChem and converted to the mol2 format using the Open Babel GUI software. The compound structure was subjected to energy minimization calculations based on the Tripos force field using SYBYL 2.1.1. The pdb files of 111 potential target proteins based on aloe emodin were downloaded from the SuperPred website on RCSB:PDB. Aloe emodin and the predicted target proteins were docked using SYBYL 2.1.1, and 5 targets with score >5.0 were selected for further analysis.

2.14. Drug affinity responsive target stability (DARTS) experiment

Caco-2 cells transfected with FFAR1-flag pcDNA3.1 plasmids for 48 h was extracted by ice-cold RIPA buffer. The protein solutions were diluted by TNC buffer (50 mmol/L Tris-HCl, pH 8.0, 50 mmol/L NaCl, 10 mmol/L $CaCl_2$) and treated with aloe emodin (0, 2.5, 10 and 40 μmol/L) at room temperature for 1 h. Then, the protein solutions were incubated with 40 ng/mL pronase at room temperature for 15 min. The reactions were ceased by adding protein loading buffer and Western blot was performed to analyze the level of FFAR1.

2.15. Cellular thermal shift assay (CETSA)

Lysate of Caco-2 cells transfected with FFAR1-flag pcDNA3.1 plasmids for 48 h was treated with aloe emodin (40 μmol/L) or 0.1% DMSO for 2 h and then heated at gradually rising temperatures (from 45 to 65 °C) for 3 min. Then, solutions were cooled on ice quickly and incubated with kinase buffer. The solutions were further centrifuged at 12,000 × *g* for 20 min and protein loading buffer was added to the supernatant for elution. Western blot was carried out to detect the level of FFAR1.

2.16. Western blot

Total proteins from cells or tissues were isolated by RIPA buffer (Beyotime, China) on ice. Nuclear proteins were extracted using NE-PER Nuclear and Cytoplasmic Extraction Reagents (Thermo Scientific). BCA Protein Assay Kit (Thermo Scientific) was used to determine the concentration of proteins. Equal amounts of proteins (10−30 μg) of each group were performed by the standard protocol of Western blot.

2.17. Immunoprecipitation

For endogenous proteins immunoprecipitation, the sample was incubated with the antibody or IgG at 4 °C for 12 h, then Protein A/G Agarose (70−100 μL) was added to each sample. The lysate beads mixture was incubated at 4 °C under rotary agitation for 4 h. Immunocomplexes were washed 3 times with 1 mL of lysis buffer and then detected by Western blot.

2.18. Enzyme-linked immunosorbent assay (ELISA)

The blood of mice was let stand for 2 h and centrifuged at 1500 × *g* for 15 min to obtain serum. The samples above were analyzed for cytokine concentration with ELISA kits according to the manufacturer's (DAKEWE) protocol.

2.19. RNA isolation and quantitative reverse transcription PCR (RT-qPCR)

For RT-qPCR analysis, the cells or tissues were lysed in Trizol reagent to extract total RNA, followed by reverse transcription with HiScript II 1st Strand cDNA Synthesis Kit (Vazyme Biotech, China). Real-Time PCR was performed using Hieff UNICON®

qPCR SYBR Green Master Mix (Yeasen, China). The profile of thermal cycling consisted of initial denaturation at 95 °C for 2 min, and 40 cycles at 95 °C for 15 s and 60 °C for 30 s. All primers used for qPCR analysis were synthesized by HuanGen Biotech (Shanghai, China). β-Actin or 18S rRNA was used as an internal control. All the qPCR primer sequences used in this study are listed in Table S1.

2.20. Single cell sequencing analysis

The expression matrix data from GSE116222[26] were created as a Seurat object using the Seurat package in R. Quality control was performed based on mitochondrial gene ratio and erythrocyte ratio. Cells were divided into 13 clusters after dimensionality reduction using uniform manifold approximation and projection for dimension reduction (UMAP). LRCs, ISCs and TA cells were further divided based on the original study. The proportions of EECs and LRCs to all intestinal epithelial cells were calculated, respectively. The expression of SOX9 in different cell clusters and different groups was calculated.

2.21. Laser capture microdissection (LCM)

Colon tissue was OCT-embedded, frozen sectioned and stained for immunofluorescence. An approximate 50 μm × 50 μm area of the SOX9 positive region on the section was cut and collected using a laser cutting microscope (PALM MicroBeam, Zeiss). Samples were then lysed using Tirzol and subjected to RT-qPCR assay.

2.22. Transcription factor (TF) prediction

We utilized the Rcis Target package in R to annotate the motifs of differentially expressed genes (DEGs) between the vehicle group and the aloe emodin (40 mg/kg) group and predict transcription factors (TFs) that bind to these motifs. Then, we used the ReMap Chip-seq database and the JASPAR website to identify TFs that could potentially bind to the promoter region (−2000 to 0) of the mouse SOX9 gene. A total of 21 predicted TFs were identified by aggregating three distinct sets of shared TFs.

2.23. Gene set enrichment analysis (GSEA) and correlation analysis of datasets

RNA-seq results of colonic epithelial cells from colitis mice and the clinical data from GSE100833 datasets[27] were subjected to standard GSEA and correlation analysis using R (version 4.1.2). Nominal *P*-values are shown.

2.24. Quantification and statistical analysis

Statistical analysis was done by GraphPad Prism 7. Unless otherwise indicated, data are represented as mean ± standard deviation (SD). Differences in the quantitative data were analyzed using 2-tailed unpaired *t*-test between two groups, and one-way analysis of variance (ANOVA) followed by Bonferroni *post hoc* test for more than two groups. N.S. represents no significance (ns), and $*P < 0.05$, $**P < 0.01$ and $***P < 0.001$ were considered significance of difference.

3. Results

3.1. Screening of active compounds in rhubarb for mouse colitis

According to the content of the components detected in rhubarb[28], we selected five free anthraquinones (emodin, aloe emodin, chrysophanol, rhein, and physcione), four stilbene analogues (piceatannol, rhapontigenin, desoxyrhapontigenin and rhaponticin) and sennoside A, the most potent laxative agent in rhubarb (Fig. 1A), for oral administration at 20 mg/kg/day in DSS-induced colitis. The results of body weight changes showed that emodin (∼ −7.52%), aloe emodin (∼ −5.98%) and piceatannol (∼ −9.31%) effectively inhibited weight loss in colitis mice (∼ −15.81%) at day 7 (Fig. 1B). Emodin, aloe emodin, chrysophanol, rhein, piceatannol and desoxyrhapontigenin significantly relieved colonic shortening in mice with colitis (Fig. 1C). RT-qPCR results showed that emodin, aloe emodin, chrysophanol and piceatannol significantly inhibited the mRNA expression of pro-inflammatory cytokines including*Il1b*, *Il6*, *Tnfa*, *Il17a*, and *Il12p40* in colons. The most significant decrease in inflammatory cytokines was observed in the aloe emodin group (Fig. 1D). We selected aloe emodin for further analysis after considering body weight, colonic length, and inflammatory cytokines expression. We characterized and identified the aloe emodin used in the study. Ultra-high performance liquid chromatography with quadrupole time-of-flight mass spectrometry (UPLC−Q-TOF-MS)/MS showed mass spectrometry fragmentation peaks consistent with previous study[29], and the high-resolution electrospray ionization mass spectrometry (HR-ESI-MS) spectrum showed that the purity of aloe emodin was close to 100% after removing the solvent peaks (Supporting Information Fig. S1A and S1B).

3.2. Aloe emodin ameliorates inflammatory response in mice colitis

Pharmacodynamic experiments of oral administration of aloe emodin in multiple dose groups showed that aloe emodin treatment after the onset of DSS-induced colitis in mouse model (Day 4) promoted weight restoration, reduced DAI and alleviated colon shortening (Fig. 2A−C). FITC-dextran permeability assays showed that aloe emodin at 20 and 40 mg/kg significantly improved the integrity of the intestinal barrier (Fig. 2D). H&E staining showed that aloe emodin effectively alleviated inflammatory cell infiltration and crypt structure loss (Fig. 2E). Consistently, the increased levels of pro-inflammatory cytokines in serum (Fig. 2F) and tissues (Fig. 2G) were significantly ameliorated in the 20 and 40 mg/kg aloe emodin groups. Overall, aloe emodin had a dose-dependent therapeutic effect on the DSS model, with 40 mg/kg aloe emodin outperforming 5-aminosalicylic acids (5-ASA). Different IBD models only fit the characteristics of human IBD partly[19], so we also evaluated the pharmacodynamics of aloe emodin in TNBS-induced models. As shown in Supporting Information Fig. S2A, 40 mg/kg aloe emodin promoted the recovery of body weight. On the 3rd day with the most severe colitis in mice, aloe emodin at 20 and 40 mg/kg showed a significant alleviating effect (Fig. S2B), eventually showing a restorative effect on colonic shortening and permeability (Fig. S2C and S2D). Consistently, inflammatory cell infiltration and colonic patch

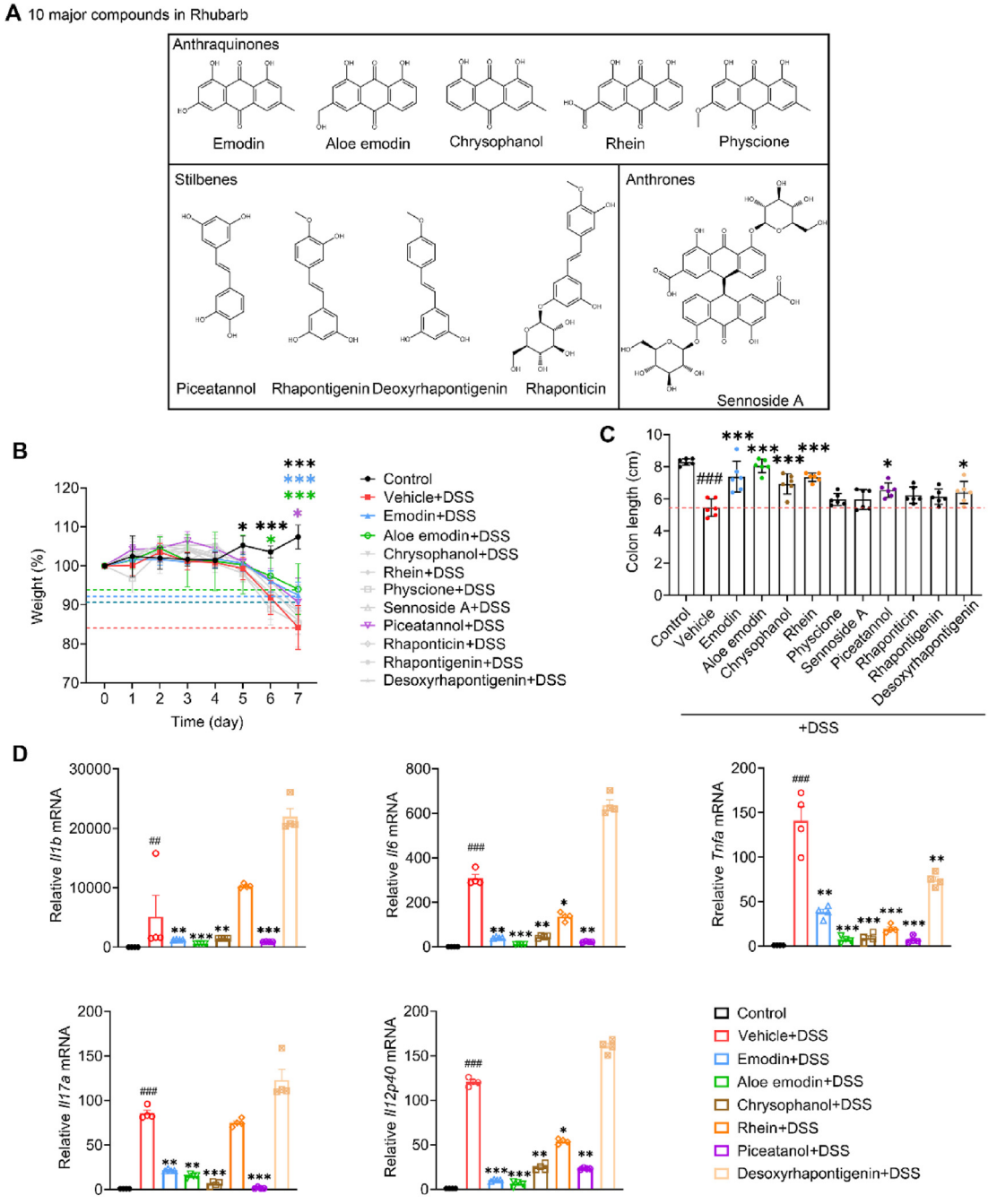

Figure 1 Screening of active compounds in rhubarb for mice colitis. (A) Chemical structure formulas of the ten main components of rhubarb. (B) Changes in body weight of mice in each group ($n = 6$). The mice were treated with 3% DSS for 7 days. Compounds (20 mg/kg/day) were given intragastrically every day. (C) The colon length of mice treated with DSS in each group on Day 7. (D) Relative mRNA levels of proinflammatory cytokines in the colon tissue measured by RT-qPCR. Data are expressed as mean ± SD. Data of 1B were compared by two-way ANOVA followed by Bonferroni *post hoc* test; $^{*}P < 0.05$, $^{**}P < 0.01$ and $^{***}P < 0.001$. Data of 1C and 1D were compared by one-way ANOVA followed by Bonferroni *post hoc* test; $^{\#\#\#}P < 0.001$ *vs* Control group; $^{*}P < 0.05$, $^{**}P < 0.01$, $^{***}P < 0.001$ *vs* Vehicle group.

hypertrophy caused by TNBS were significantly reduced by aloe emodin (Fig. S2E). ELISA and RT-qPCR results suggested a significant inhibitory effect of 40 mg/kg aloe emodin on levels of pro-inflammatory cytokines in serum (Fig. S2F) and colonic tissue (Fig. S2G). Overall, aloe emodin also provided dose-dependent remission in the TNSB model, where 40 mg/kg aloe emodin exhibited efficacy similar to that of 5-ASA.

3.3. Aloe emodin interferes with the differentiation of precursor cells to early EECs

RNA-seq data from intestinal tissues showed that the differentially expressed genes (DEGs) between aloe the emodin (40 mg/kg) group and vehicle group were enriched in the pancreatic secretion, linoleic acid metabolism and prolactin signaling pathway annotated by the

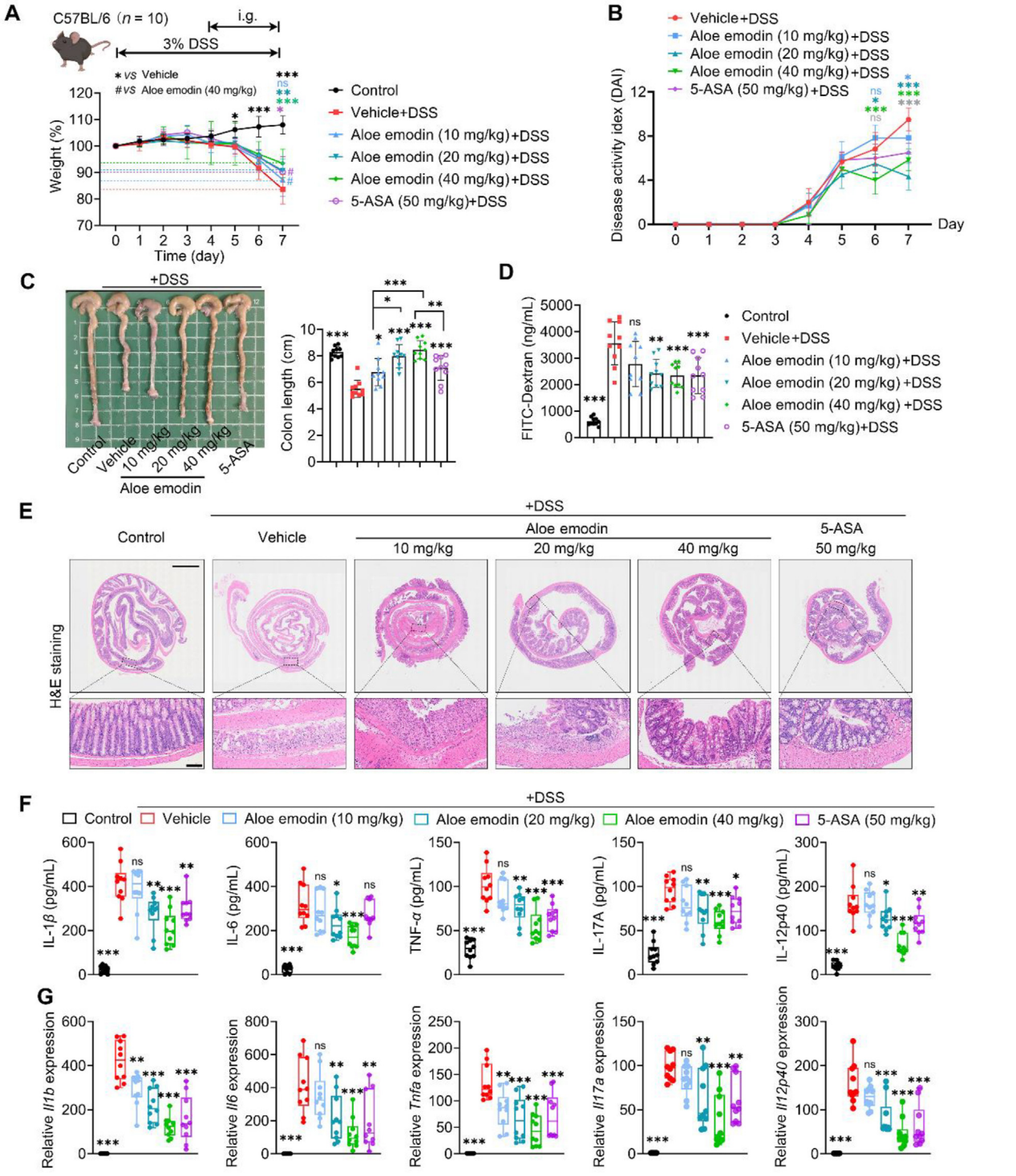

Figure 2 Aloe emodin ameliorated inflammatory response in mice colitis. (A) Body weight change of mice subjected to colitis induction with 3% DSS for 7 days ($n = 10$ per group). Mesalazine (50 mg/kg/day) or aloe emodin (10/20/40 mg/kg/day) were given intragastrically from Day 4. (B) Disease activity index (DAI) score of each group. (C) The colon length of each group mice treated with DSS on Day 7. (D) The intestinal permeability *in vivo* was evaluated using FITC-Dextran. (E) Representative H&E staining images of DSS-induced mice on Day 7. Scale bars, 2 mm (top panel). Scale bars, 100 μm (bottom panel). (F) The concentration of proinflammatory cytokines in mouse serum was measured by ELISA. (G) Relative mRNA levels of proinflammatory cytokines in the colon tissue measured by RT-qPCR. Data are represented as means ± SD. Data of 2A is compared by two-way ANOVA followed by Bonferroni *post hoc* test. DAI of each day (2B) is compared by Kruskal−Wallis test followed by Dunn's *post hoc* test. Other data are compared by one-way ANOVA followed by Bonferroni *post hoc* test. Not significant (NS), $^{\#}P < 0.05$ *vs* Aloe emodin (40 mg/kg) group; $^{*}P < 0.05$, $^{**}P < 0.01$, $^{***}P < 0.001$ *vs* Vehicle group.

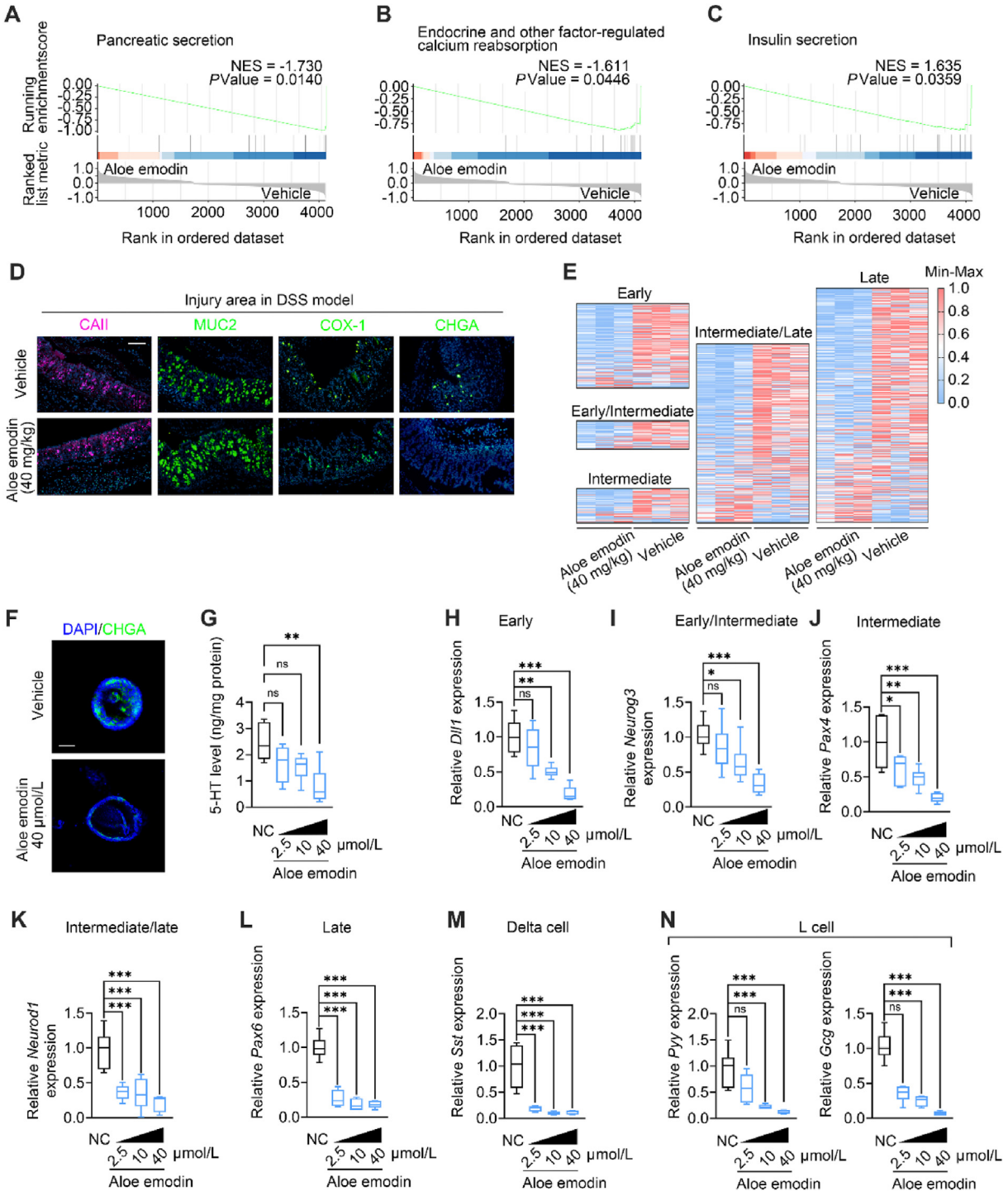

Figure 3 Aloe emodin interferes with the differentiation of precursor cells to early EECs. (A–C) GSEA on bulk RNA-seq data from colon tissue, comparing the Aloe emodin (40 mg/kg) group to the vehicle group ($n = 3$ per group). (D) Immunofluorescent staining of differentiation markers (CAII for absorptive colonocytes, MUC2 for goblet cells, CHGA for enteroendocrine cells, COX-1 for tuft cells) in colon sections. Scale bars, 100 μm. (E) Relative expression of time-resolved list of transcriptional regulators of EECs at different stages of differentiation in aloe emodin (40 mg/kg) group vs vehicle group ($n = 3$ per group). (F) Immunofluorescent staining of CHGA in colonic organoids (on the 5th day of *in vitro* culture) with or without aloe emodin treatment (40 μmol/L) for 24 h. Scale bars, 50 μm. (G) The concentration of 5-HT in colonic organoids with or without aloe emodin treatment for 24 h was measured by ELISA kit ($n = 6$ per group). NC, negative control. (H–L) Relative mRNA levels of markers of endocrine cell linage at different stages (*Dll1*, *Neurog3*, *Pax4*, *Neurod1 and Pax6*) in organoids measured by RT-qPCR ($n = 6$ per group). (M, N) Relative mRNA levels of hormone from delta cells (*Sst*) and L cells (*Pyy* and *Gcg*) in organoids measured by RT-qPCR ($n = 6$ per group). Data are represented as mean ± SD. Data are compared by one-way ANOVA followed by Bonferroni *post hoc* test. Not significant (ns), $^{*}P < 0.05$, $^{**}P < 0.01$ and $^{***}P < 0.001$.

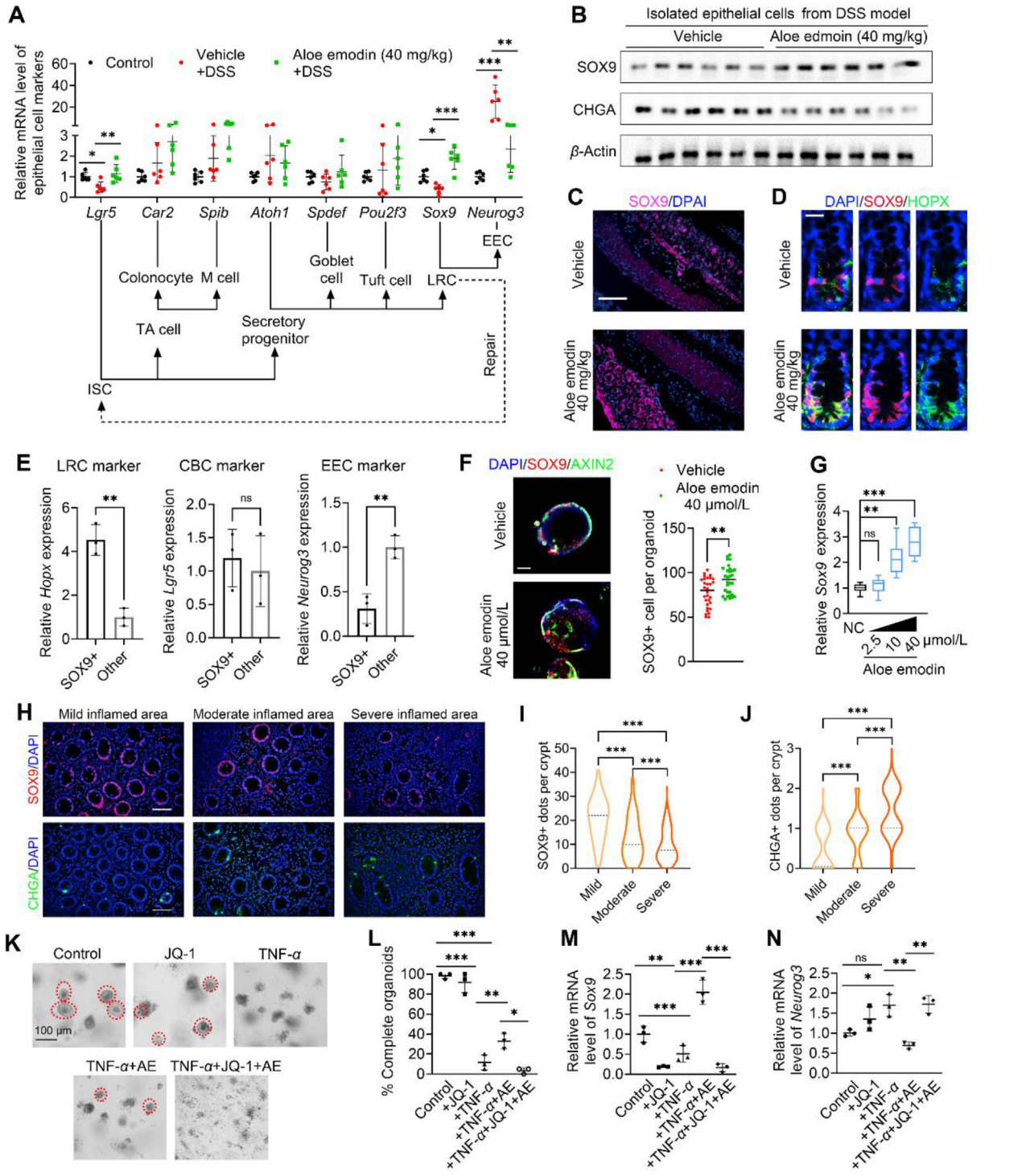

Figure 4 SOX9-mediated arrest of LRC differentiation is required for aloe emodin to promote mucosal repair. (A) Relative mRNA levels of epithelial cell markers in sorting colon epithelial cells (CD45-EPCAM$^+$) isolated from DSS-induced mice (n = 6 per group) measured by RT-qPCR. (B) Representative immunoblots of SOX9 and CHGA protein in isolated epithelial cells from DSS-induced mice (n = 6 per group). (C) Immunofluorescent staining of SOX9 in colon sections from vehicle group *vs* aloe emodin (40 mg/kg) group in DSS-induced colitis. Scale bars, 100 μm. (D) Immunofluorescent staining of SOX9 and HOPX in longitudinal sections of crypts from vehicle group *vs* aloe emodin (40 mg/kg) group. Scale bars, 20 μm. (E) Relative mRNA levels of *Hopx* (LRC marker), *Lgr5* (CBC marker), and *Neurog3* (ECC marker) in SOX9$^+$ cells-enriched regions and SOX9-regions separated by LCM. (F) Left panel: Immunofluorescent staining of AXIN2 and SOX9 in colonic organoids (on the 5th day of *in vitro* culture) with or without aloe emodin treatment (40 μmol/L) for 24 h. Scale bars, 50 μm. Right panel: The SOX9$^+$ cells count in organoids. (G) Relative mRNA levels of *Sox9* in the in organoids with or without aloe emodin treatment measured by RT-qPCR. (H) Immunofluorescent staining of SOX9 and CHGA in inflamed intestinal areas with different degrees from CD patients. Scale bars, 50 μm. (I, J) The counts of SOX9$^+$ and CHGA$^+$ cells per crypt (100 crypts for each group) in inflamed areas with different degrees. (K, L) Representative images

Kyoto encyclopedia of genes and genomes (KEGG) (Supporting Information Fig. S3A). GSEA showed that pancreatic secretion, endocrine and other factor-regulated calcium reabsorption and insulin secretion gene sets were enriched in the vehicle group compared to the aloe emodin (40 mg/kg) group, suggesting that aloe emodin down-regulated intestinal secretory cell-related functions *in vivo* (Fig. 3A–C). We performed immunofluorescence staining for different types of secretory epithelial cells' markers in selected injury areas (defined by the presence of inflammatory cell infiltration and intact crypt) for quantitative analysis. The results showed that aloe emodin administration significantly suppressed the number of EECs ($CHGA^+$), while it had no effect on the number of absorptive cells ($CAII^+$), goblet cells ($MUC2^+$) and tuft ($COX1^+$) cells (Fig. 3D and Fig. S3B), supporting our finding from GSEA analysis. We used a previously reported time-resolved list of transcriptional regulators of EECs for discriminating the effect of aloe emodin on EECs at different stages of differentiation[30]. The results showed that most of the regulators of each stage were down-regulated in aloe emodin group, indicating that aloe emodin might inhibit the EEC maturation from the early stage (Fig. 3E). Then, we treated colon organoids with 2.5–40 μmol/L aloe emodin for 24 h before the emergence of mature $CHGA^+$ EECs (~Day 5) to test whether aloe emodin has a direct effect on epithelial cell differentiation. CHGA staining and 5-HT level of colon organoids indicated that aloe emodin suppressed the differentiation of epithelial cell lineage to enteroendocrine cells (Fig. 3F and G). Consistent with RNA-seq data of mouse intestinal tissue, RT-qPCR determining EEC time-resolved markers suggested that aloe emodin suppressed the expression of EECs markers in all periods including terminally differentiated delta cells and L cells (Fig. 3H–N). These data suggest that aloe emodin alters the differentiation of precursor cells to early EECs.

3.4. *SOX9-mediated arrest of LRC differentiation is required for aloe emodin to promote mucosal repair*

To clarify the exact mechanisms by which aloe emodin affects epithelial cell differentiation, we obtained mouse purified colonic epithelial cells by EDTA digestion combined with $EPCAM^+CD45^-$ immunomagnetic bead sorting and measured the marker gene expression of different epithelial cells differentiated from ISCs. Interestingly, *Sox9* and *Lgr5* expression was significantly downregulated in colitis and rescued by aloe emodin treatment, which is in complete contrast to the trend of *Neurog3* expression (Fig. 4A). Consistently, aloe emodin also up-regulated SOX9 protein levels and down-regulated CHGA protein levels in sorting epithelial cells (Fig. 4B, Supporting Information Fig. S4A). Immunofluorescence staining showed that aloe emodin upregulated the number of $SOX9^+$ cells in the injury area (Fig. 4C and Fig. S4B) and there was a significant negative correlation between the numbers of $SOX9^+$ cells and $CHGA^+$ cells regardless of subgroup ($r = -0.5056$) (Fig. S4B). High SOX9 expression is one of the characteristics of LRCs, also known as quiescent "+4" cells, or reserve ISC (rISCs)[8,9]. SOX9 staining of longitudinal sections of crypts showed that aloe emodin enlarged $SOX9^+$ cell population located close to the theoretical location of LRCs and co-expressed homeodomain-only protein (HOPX) which is an LRC marker (Fig. 4D). Separation of $SOX9^+$ cells-enriched regions using laser capture microdissection showed that the transcriptional profile of the $SOX9^+$ regions was close to that of the LRC compared to the $SOX9^-$ region (Fig. 4E). These data suggest that the increased $SOX9^+$ cells caused by aloe emodin are LRCs. Data from cultured mouse colonic organoids also showed that aloe emodin upregulated the number of $SOX9^+$ LRCs and *Sox9* expression (Fig. 4F–G). Interestingly, aloe emodin did not increase the number of $AXIN2^+$ cells (CBCs) *in vitro*, suggesting that the upregulation of *Lgr5* observed in aloe emodin-treated colitis mice was due to the transformation of the increased SOX^+ LRCs rather than the self-amplification of CBCs. Notably, $SOX9^+$ LRCs are precursor cells for EECs[3] and an alternate source of $LGR5^+$ CBCs in epithelial damage[8,9]. Assuming that the number of LRC population is constant, selection for LRC differentiation to CBCs or EECs in colitis might have an impact on epithelium repair. To understand the impact of this differentiation trend on CD, we analyzed transcriptome profiling data (GSE100833 dataset) from active CD patients[27]. As shown in Fig. S4C and S4D, SOX9 expression was significantly downregulated and Neurogenin3 (NEUROG3) expression was significantly upregulated in biopsy samples from inflamed area compare to non-inflamed areas. Staining of clinical samples also showed that, as inflammation increased, $SOX9^+$ LRCs significantly decreased, whereas $CHGA^+$ EECs significantly increased in the colonic crypts from CD patients (Fig. 4H–J). Results after further clustering of undifferentiated cells on previous single-cell sequencing data (GSE116222 dataset)[26] showed that the number of EECs was higher in inflamed areas than in healthy control and non-inflamed area, whereas the number of LRCs was lower in inflamed regions than in non-inflamed regions (Fig. S4E–S4H). Moreover, SOX9 expression was significantly higher in EECs from non-inflamed areas than in inflamed areas (Fig. S4I). According to these data, we propose a conjecture that downregulated SOX9 expression levels in inflammation leads to a tendency of LRC to over-differentiate toward EEC. We treated organoids with tumor necrosis factor alpha (TNF-α, 10 ng/mL) to simulate colonic inflammation and observed the apoptosis of the organoids[31]. As shown in Fig. 4K and L, aloe emodin significantly suppressed organoid apoptosis induced by TNF-α. Moreover, aloe emodin partially reversed the TNF-α-induced decrease in *Sox9* expression and increased *Neurog3* expression (Fig. 4M and N). However, all the aloe emodin-induced effects were blocked by SOX9-CRISPR knock out (ko) and JQ-1 which downregulated SOX9 transcription as an epigenetic inhibitor (Fig. S4J–M and Fig. 4K–N)[32]. These data confirm our conjecture and suggest that SOX9-mediated arrest of LRC differentiation is required for aloe emodin to promote mucosal repair.

3.5. *FOXO1 is the key transcription factor in the up-regulation of SOX9 expression by aloe emodin*

We further inquired the possible signaling pathways mediating the aloe emodin-induced upregulation of SOX9 expression.

of organoids and quantification of complete organoids stimulated by TNF-α (10 ng/mL) with or without aloe emodin (AE) treatment (40 μmol/L) or JQ-1 (SOX9 inhibitor) treatment. (M, N) Relative mRNA levels of *Sox9* and *Neurog3* in organoids stimulated by TNF-α (10 ng/mL) with or without aloe emodin treatment (40 μmol/L) or JQ-1 (1 μmol/L) treatment was measured by RT-qPCR. Data are represented as means ± SD. Data of 4E and 4F (right panel) are compared by two-sided unpaired *t*-test. Other data are compared by one-way ANOVA followed by Bonferroni *post hoc* test. Not significant (ns), $^*P < 0.05$, $^{**}P < 0.01$ and $^{***}P < 0.001$.

Firstly, we identified the transcription factor (TF) binding motifs enriched in the DEGs between aloe emodin and vehicle treated mice colon using RcisTarget package. As shown in Fig. 5A, 50 TFs could theoretically bind to these motifs of DEGs, suggesting that aloe emodin might modulate the expression of SOX9 and other DEGs *via* regulating these TFs. We further identified TFs that may bind to a 2000 bp sequence upstream of the SOX9 gene promoter *via* JASPAR TFBS and ReMap ChIP-seq database (Fig. 5B). Collectively, the predictions of the three analyses indicated that 21 TFs might be modulated by aloe emodin ultimately upregulating SOX9 expression (Fig. 5C). We further found that there were 6 TFs including FOXO1, FOS, JUNB, FOXA1, POU5F1 and RXRA correlating significantly ($P < 0.001$) with SOX9 expression in the CD (Fig. 5D and Supporting Information Fig. S5A). Next, we hypothesized that the modulated TF could upregulated SOX9 expression and downregulated NEUROG3 expression. CD patients (GSE100833)[27] were grouped into four groups according to the median *SOX9*/*NEUROG3* expression level. As shown in Fig. S5B, pyruvate metabolism, transforming growth factor-beta (TGF-β) and FOXO signaling pathways were enriched in the *SOX9*^{high}*NEUROG3*^{low} group of patients. In contrast, PPAR, autophagy and NF-κB signaling pathways were enriched in patients in the *SOX9*^{low}*NEUROG3*^{high} group. Together, these analyses revealed that FOXO1 was the TF with the highest potential to mediate the aloe emodin-induced upregulation of SOX9. It was demonstrated by the fact that the inhibitor of FOXO1 (AS1842856) blocked the regulation of aloe emodin on the expression of *SOX9* and *NEUROG3* (Fig. 5E and F). Besides, FOXO1-CRISPR knockout (ko) organoids also exhibited over-differentiation towards EECs, which could not be reversed by aloe emodin (Fig. 5G). Next, we used the JASPAR database to predict the binding of FOXO1 and 2000 bp gene sequences upstream of SOX9, and the results showed that FOXO1 can bind to multiple sequences upstream of SOX9 (Fig. S5C). Considering the length and specificity of the probes, we selected the binding sequence with the second highest predicted score for DNA pull-down experiment, and the results showed that the probe synthesized according to the upstream position (−1313 to −824) of *SOX9* bind to FOXO1 (Fig. 5H). CHIP-qPCR experiments further identified the binding site at the −1095 to −824 site which was closer to the predicted −1065 to −1052 site, indicating that FOXO1 could bind to the predicted sequence upstream of FOXO1 and could be enhanced by aloe emodin (Fig. 5I). Collectively, we identified FOXO1 as the key transcription factor mediating the up-regulation of SOX9 expression by aloe emodin.

3.6. *Aloe emodin promotes FOXO1 nuclear translocation via inhibiting its phosphorylation*

The activity of FOXO1 is influenced by its expression abundance, post-translational modifications (mainly including phosphorylation and acetylation), nuclear-cytoplasmic shuttling dynamics, and subcellular localization[33]. Western blots showed that aloe emodin upregulated nuclear translocation of FOXO1 (Fig. 6A, Supporting Information Fig. S6A and S6B), and similar results were obtained by immunofluorescence staining (Fig. 6B and C). However, aloe emodin did not affect the protein and mRNA abundance of FOXO1 (Fig. 6A and D, Fig. S6A). Further results showed that the protein phosphatase inhibitor (Okadaic acid) rather than histone deacetylase inhibitor (trichostatin A, TSA) or sirtuin inhibitor (NAM) blocked the upregulation of SOX9 expression induced by aloe emodin (Fig. 6E), which suggested that aloe emodin upregulated SOX9 expression *via* affecting the phosphorylation modifications instead of acetylation. AKT, extracellular signal-regulated kinase (ERK1/2), and casein kinase 1 (CK1α) induce the phosphorylation and nuclear export of FOXO1[34]. Our result showed that AKT activator (SC79) instead of ERK1/2 or CK1α activator (Ro677476, SSTC3) blocked aloe emodin-induced upregulation of SOX9 expression (Fig. 6E), suggesting that aloe emodin upregulated SOX9 expression *via* altering the activity of AKT. AKT directly phosphorylates FOXO1 on three different sites (Thr24, Ser256, Ser319), leading to its transcriptional inactivation by nuclear export[35]. Our results supported that aloe emodin dose-dependently reduces AKT-induced phosphorylation (at Ser256) of FOXO1 (Fig. 6F and Fig. S6C). In addition, the application of phosphoinositide 3-kinase (PI3K) inhibitor (ETP-45658) or an AKT inhibitor (Capivasertib) effectively promoted *Sox9* expression (Fig. S6D). AKT-phosphorylated FOXO1 binds to the 14-3-3 chaperone protein, blocking FOXO1 nuclear translocation signal the nuclear translocation signal of FOXO1 and causing FOXO1 to be bound in the cytoplasm[35,36]. Immunofluorescence images and co-immunoprecipitation showed that aloe emodin weakened the interaction of FOXO1 and 14-3-3σ (Fig. 6G, H, and Fig. S6E). Further, overexpression of FOXO1-flag on FOXO1-CRISPRko Caco-2 cells rescued aloe emodin-induced SOX9 high-expression, which is consistent with nuclear FOXO1 (Fig. 6I and Fig. S6F). In conclusion, our data suggested that aloe emodin decreased the AKT-induced phosphorylation of FOXO1 and promoted FOXO1 entry into the nucleus to upregulate SOX9 transcription.

3.7. *Aloe emodin targets FFAR1 to inhibit G$\beta\gamma$/AKT/p-FOXO1 signaling pathway*

We obtained 5 targets of aloe emodin with high possibility based on the result from the SuperPred website combined with the SYBYL-X software docking score (>5.0) (Fig. 7A). Correlation analysis showed that only the free fatty acid receptor 1 (FFAR1/GPR40) was significantly correlated with SOX9/NEUROG3 balance (Fig. 7B and C). As shown in Fig. 7D, aloe emodin was embedded into the pocket around the residues VAL1094, ASP1092, ARG1095 and THR1155 of FFAR1. Results of the DARTS experiment revealed that proteolysis of FFAR1 by protease was significantly decreased by the presence of aloe emodin (Fig. 7E), indicating that aloe emodin binding contributed to the increased protease-resistant of FFAR1. Consistently, CETSA result showed that aloe emodin increased the thermal stability of FFAR1. According to the blots and melting curves, we observed a significant melting temperature shift from 52.76 °C (DMSO) to 57.70 °C (aloe emodin) (Fig. 7F). Linoleic acid is an endogenous ligand of FFAR, which can explain why aloe emodin caused linoleic acid pathway altered in KEGG enrichment (Fig. S3A).

We used linoleic acid[37] and TAK-875 (a selective agonist of FFAR1)[38] to confirm the effect of aloe emodin on FFAR1. RT-qPCR and Western blot data showed that both linoleic acid and TAK-875 had opposite effects to aloe emodin on SOX9/NEUROG3 expression levels (Fig. 7G), and phosphorylation (Ser256) and nuclear translocation of FOXO1 (Fig. 7H). However, TAK-875 reversed the effects of aloe emodin, but linoleic acid did not. Virtual docking results showed that TAK-875 was binding to the different pocket of FFAR1 (Supporting Information Fig. S7A). As shown in Fig. S7B, aloe emodin could suppress intracellular inositol monophosphate

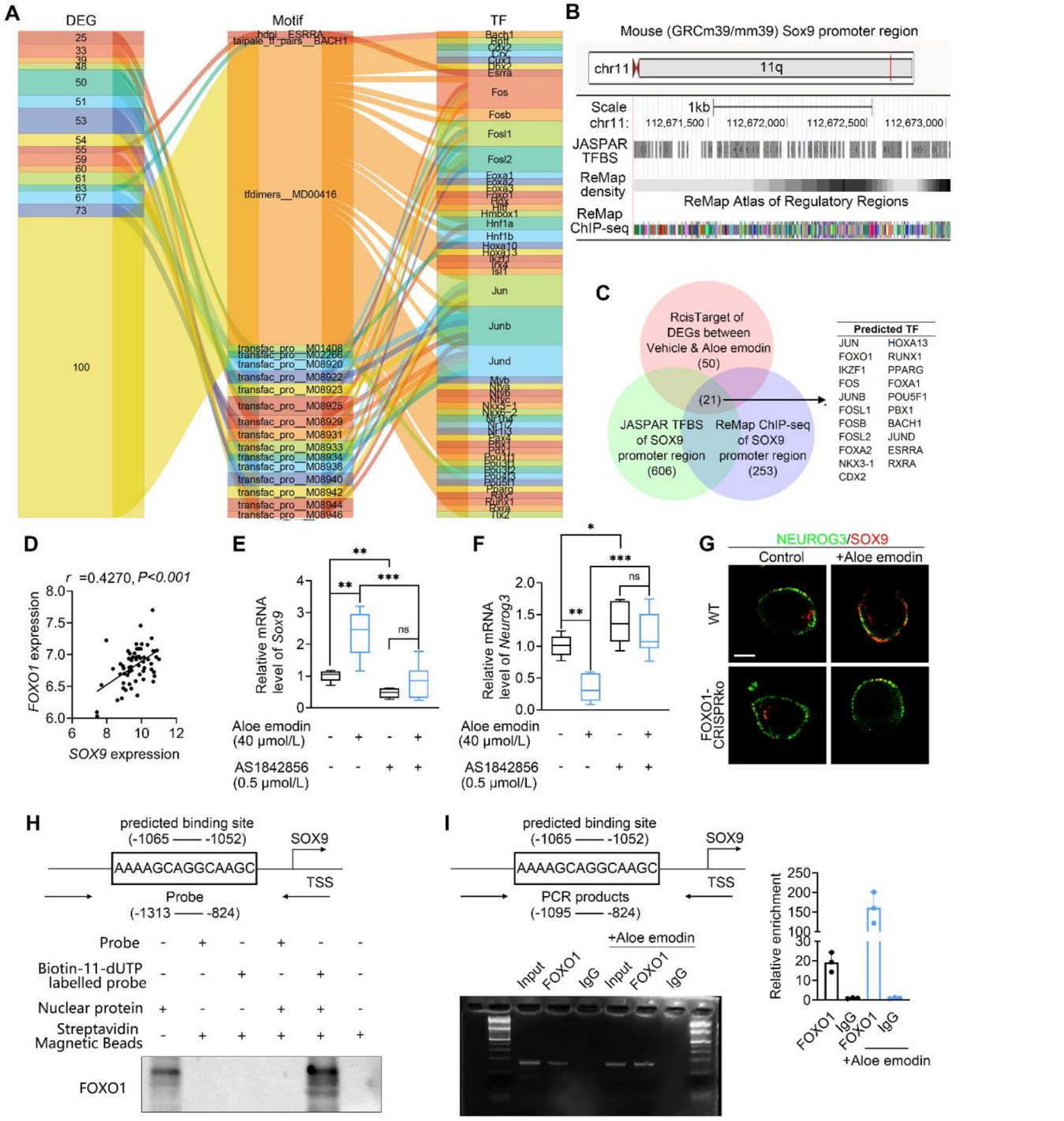

Figure 5 FOXO1 is the key transcription factor in the up-regulation of SOX9 expression by aloe emodin. (A) TF prediction based on DEGs (from bulk RNA-seq of colon tissue) between vehicle group and aloe emodin (40 mg/kg) group by RcisTarget tool. (B) JASPAR TFBS and ReMap ChIP-seq of SOX9 promoter region on UCSC website. (C) Wayne plot and list of predicted TFs. (D) Correlation analysis by Spearman between *SOX9* and *FOXO1* mRNA expression in inflamed intestine areas from CD patients ($n = 69$) of GSE100833 dataset. (E, F) Relative mRNA levels of *Sox9* and *Neurog3* in organoids with or without FOXO1 inhibitor (AS1842856) or aloe emodin treatment for 24 h measured by RT-qPCR. (G) Immunofluorescent staining of SOX9 and NEUROG3 in WT or FOXO1-CRISPRko colonic organoids with or without aloe emodin treatment (40 μmol/L) for 24 h. Scale bars, 50 μm. (H) FOXO1 bound to the SOX9 promoter indicated by DNA pull-down assay. (I) The binding activity of FOXO1 to SOX9 promoter detected by CHIP assay. Experiments of Fig. 5H and I were performed on human colonic adenoma Caco-2 cells. Data are represented as mean ± SD and analyzed by one-way ANOVA followed by Bonferroni *post hoc* test. Not significant (ns), $^{*}P < 0.05$, $^{**}P < 0.01$, and $^{***}P < 0.001$.

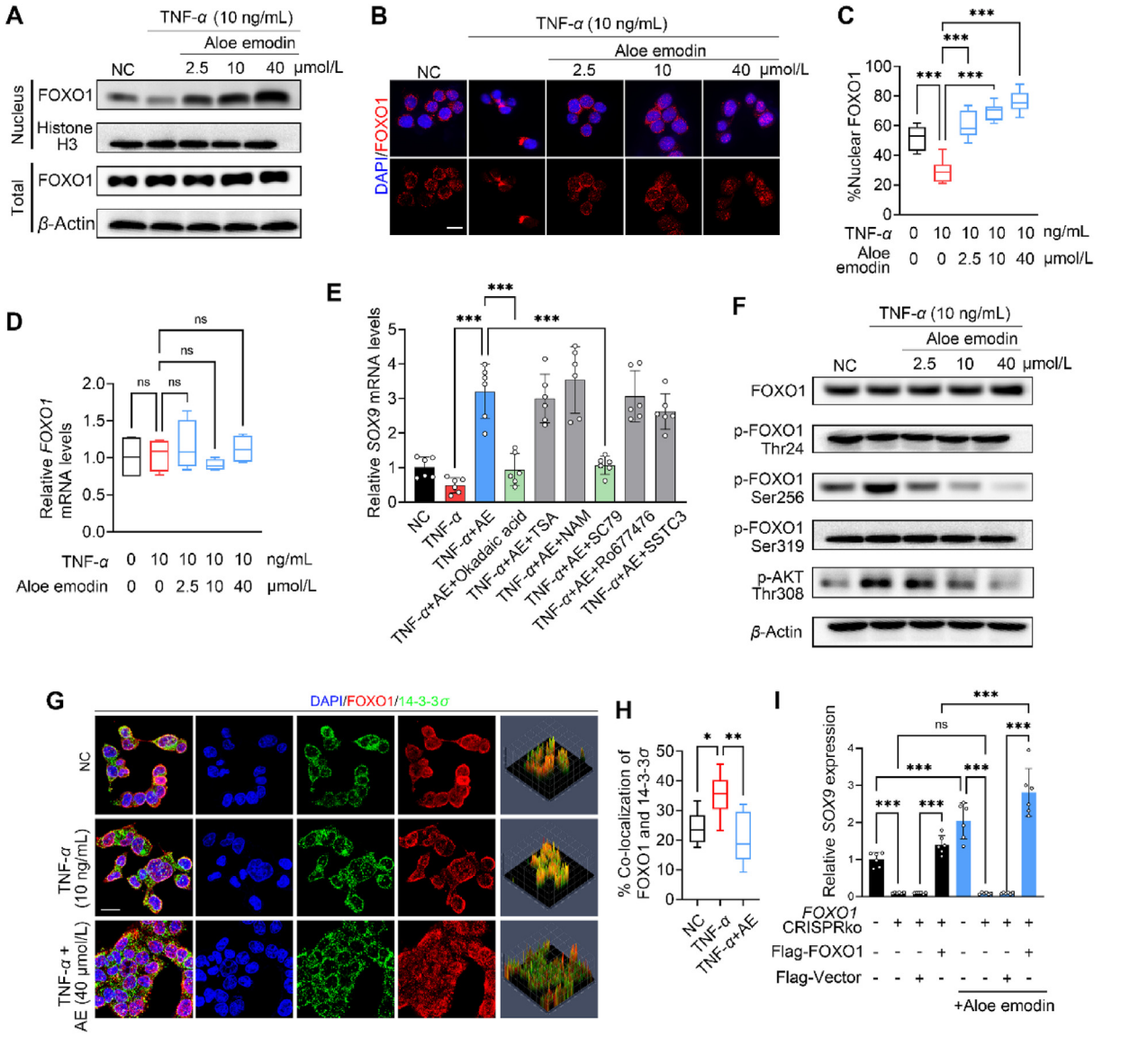

Figure 6 Aloe emodin promotes FOXO1 nuclear translocation *via* inhibiting its phosphorylation. (A) Representative immunoblots for total and nuclear proteins of FOXO1 in TNF-α-induced (10 ng/mL for 12 h) Caco-2 cells with or without aloe emodin treatment for 2 h. (B, C) FOXO1 nuclear location (2 h after aloe emodin treatment) was assessed by immunofluorescence staining and quantified by Image J. Scale bar, 20 μm. (D) Relative mRNA level of *FOXO1* with aloe emodin treatment for 6 h measured by RT-qPCR. (E) Relative mRNA level of *Sox9* with aloe emodin treatment for 6 h after inhibitors (250 nmol/L okadaic acid for protein phosphatase, 20 μmol/L TSA for histone deacetylase, 2 mmol/L NAM for Sirtuin) or activators (10 μmol/L SC79 for AKT, 200 nmol/L Ro677476 for ERK1/2 and 100 nmol/L SSTC3 for CK1α) treatment was measured by RT-qPCR. (F) Representative immunoblots for FOXO1 and phosphorylated-FOXO1 (Thr24, Ser 256 and Ser319) with aloe emodin treatment. (G, H) Immunofluorescence images of FOXO1 and 14-3-3σ staining treated with or without aloe emodin (40 μmol/L). Images were observed by confocal microscopy and colocalization was analyzed by Image J's JACop plugin. Scale bar, 20 μm. (I) WT and FOXO1-CRISPRko Caco-2 cells transfected with Flag-Vector or Flag-FOXO1 were treated with or without aloe emodin (40 μmol/L) for 6 h. The relative SOX9 expression was determined by RT-qPCR. Data are represented as mean ± SD and analyzed by one-way ANOVA followed by Bonferroni *post hoc* test. Not significant (ns), *$P < 0.05$, **$P < 0.01$, and ***$P < 0.001$.

(IP, a downstream metabolite of IP_3) production induced by linoleic acid but not TAK875 in FFAR1 expressing Caco-2 cells. The concentration for 50% of maximal inhibitory (IC_{50}) of aloe emodin on IP production by FFAR1 agonist linoleic acid (100 μmol/L) was 4.167 μmol/L, much larger than concentration for 50% of maximal effect (EC_{50}) of TAK875 (0.2148 μmol/L) (Fig. S7B and S7C). These data explained why TAK875 reversed FFAR1 inhibition by aloe emodin. This finding was further substantiated by our *in vivo* studies, where TAK875 administration reversed the protective effect of aloe emodin in the colitis model (Fig. 7I) and its regulation of Sox9/Neurog3 expression (Fig. 7J). We further investigated the phosphorylation of AKT at the Ser308 residue which decide whether AKT can phosphorylate FOXO1. The results showed that TAK875 blocked aloe emodin-induced down-regulation of p-AKT (Thr308), which suggested that FFAR1 transduces signals to FOXO1 *via* p-AKT (Thr308) (Fig. 7H). It was reported that G$\beta\gamma$

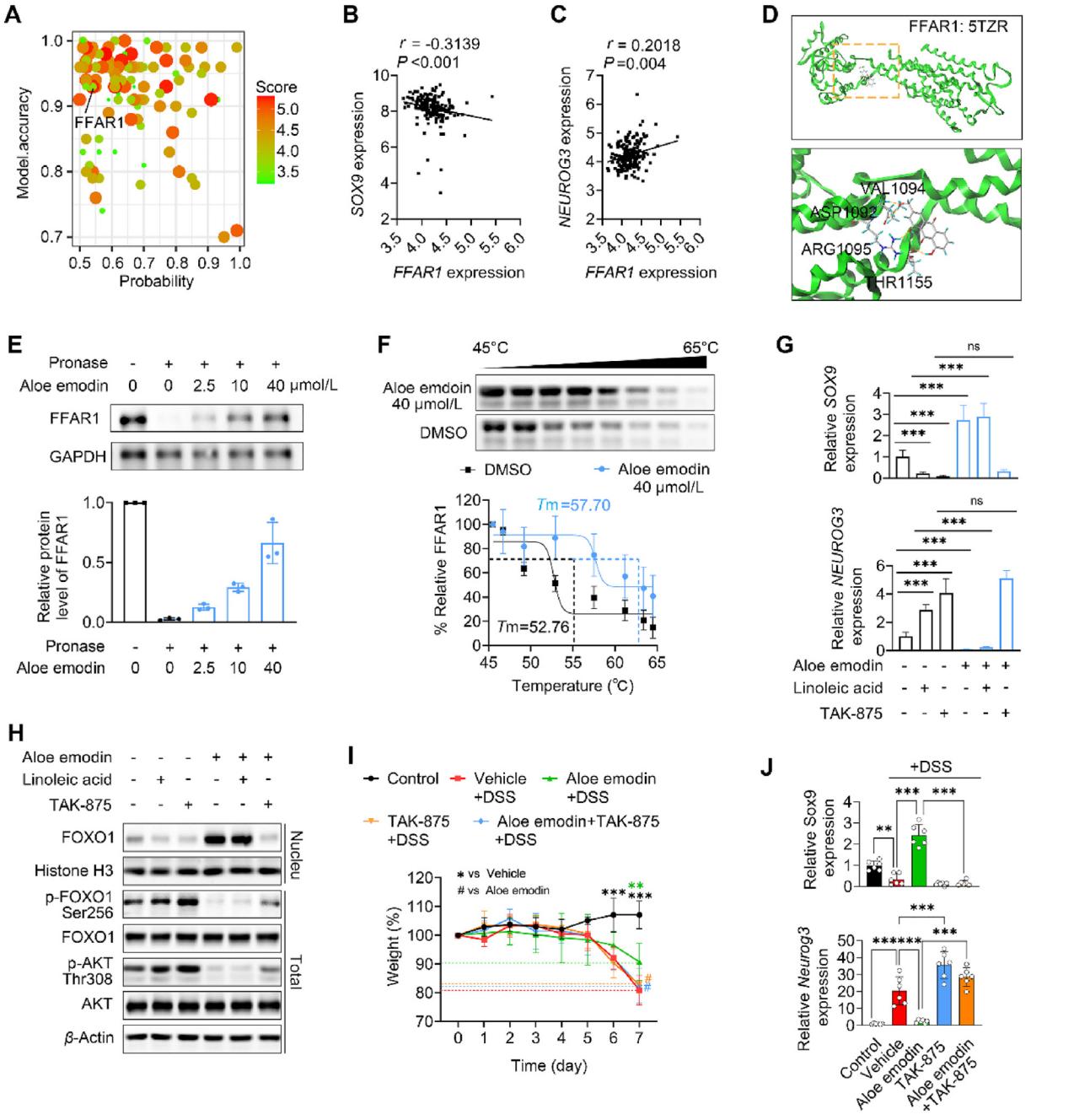

Figure 7 Aloe emodin targets FFAR1 to inhibit Gβγ/AKT/p-FOXO1 signaling pathway. (A) Predicted aloe emodin-binding targets from SuperPred website were further scored by SYBYL-X docking. Model accuracy and probability were provided by the SuperPred website, and scores were generated by SYBYL-X 2.1.1 software. (B, C) Correlation analysis by Spearman between *FFAR1* and *SOX9* (or *NEUROG3*) mRNA expression in biopsy samples from CD patients ($n = 69$) of GSE100833 dataset. (D) Modeling result of aloe emodin and FFAR1 (PDB: 4PHU). Top panel: Binding mode of aloe emodin and FFAR1. Bottom panel: a closer look of detail interactions between aloe emodin and residues of the pocket. Hydrogen bonds were shown as dotted line (yellow) between atoms. (E) Lysates from FFAR1-flag-expressing Caco-2 cells was incubated with aloe emodin (0, 2.5, 10 and 40 μmol/L) and then subjected to pronase digestion. Immunoblots using anti-flag antibody are shown. (F) CETSA was conducted with in intact FFAR1-flag-expressing Caco-2 cells with DMSO or aloe emodin treatment. Representative Western blots for the stabilization of FFAR1-flag protein under 45−65 °C are shown. The protein levels were quantified by Image J. (G) Relative mRNA levels of *SOX9* and *NEUROG3* with or without linoleic acid (100 μmol/L), TAK-875 (1 μmol/L) or aloe emodin treatment (40 μmol/L) for 6 h measured by RT-qPCR. (H) Representative immunoblots for indicated nuclear or total protein with indicated treatment for 2 h. (I) Body weight change graph of mice ($n = 6$) subjected to 3% DSS induction for 7 days. Aloe emodin (40 mg/kg/day), TAK-875 (30 mg/kg) or combination was given intragastrically from Day 4. (J) Relative mRNA levels of *Sox9* and *Neurog3* in colon epithelial cells isolated from DSS-induced mice ($n = 6$) on Day 7 measured by RT-qPCR. Data are represented as mean ± SD. Data of 7I are analyzed by two-way ANOVA followed by Bonferroni *post hoc* test. Data of 7G and J are analyzed by one-way ANOVA followed by Bonferroni *post hoc* test. Not significant (ns), $^{*}P < 0.05$, $^{**}P < 0.01$, and $^{***}P < 0.001$.

subunits, released upon activation of Gα-coupled receptors, directly interacts with PI3K to activate the PI3Kγ/p-AKT (Thr308) signaling pathway[39,40]. Our results also showed that the agonistic effect of linoleic acid was blocked by gallein but not pertussis toxin (PTX), indicating that FFAR1-driven SOX9/NEUROG3 regulation was mainly conducted by Gβγ (Fig. S7D). Previous study demonstrated that G protein-coupled receptor (GPCR) transduction to PI3K/AKT prefers using Gγ3 than other isoforms of the Gγ subunits[41]. Here, we further found a preference for the Gβ2 subunit in FFAR1-meditated down-regulation of SOX9 expression (Fig. S7E). Together, we identified FFAR1 as the target of aloe emodin and found that activated FFAR1 downregulates SOX9 expression *via* Gβ2γ3/AKT/p-FOXO1 signaling pathway, which can be blocked by aloe emodin.

4. Discussion

The epithelial layer serves as the structural foundation of the mucosal barrier. Repetitive damage to the intestinal epithelium leads to the disruption of the mucosal structure and function, acting as a key driver of IBD recurrence[42,43]. Recent research has uncovered mucosal healing as a critical therapeutic goal for the management of IBD[44,45]. Achieving complete restoration of intestinal mucosal structure and function holds the promise of sustained alleviation of clinical symptoms and reduced surgical risks for patients[2]. However, current pharmacological treatments, including 5-aminosalicylic acid (5-ASA) agents, glucocorticoids, immunosuppressants and biologic agents, do not effectively produce satisfactory results in mucosal healing, especially in CD[46,47]. These medications primarily target immune inflammation control, offering limited efficacy in epithelium repair[48]. In the mechanistic study based on the natural product aloe emodin, we found that preventing the differentiation of $SOX9^+$ LRCs to EECs might improve the epithelium reconstruction. Our data demonstrate that aloe emodin increased the self-repair capacity of organoids consisting only of epithelial cells. Previous *in vitro* experiments suggest that aloe emodin inhibit the production of inflammatory cytokines in RAW264.7 cells[49]. Thus, aloe emodin-induced anti-inflammatory *in vivo* may be the result of a mixture of epithelial barrier protection and inflammation inhibition. Our previous study showed that 5-ASA did not increase the self-renew capacity of epithelial organoids[50]. And the other laboratories also reported that the therapeutic effect of 5-ASA *in vivo* is due to its significant induction of Treg cells[51,52]. Thus, although both aloe emodin and 5-ASA ultimately reached a reduction in inflammatory cytokines *in vivo*, the mechanisms involved are different. 5-ASA and many other anti-inflammatory drugs have been found to be ineffective in many IBD patients, especially CD patients. Therefore, we aims to find active compounds that can promote mucosal repair in addition to anti-inflammation. Under physiological conditions, $LGR5^+$ CBCs are responsible for the renewal of epithelial cells, whereas in colitis self-renewal capacity of $LGR5^+$ CBCs are suppressed[4-7]. Although we observed an upregulation of *Lgr5* expression in the aloe emodin treatment group, aloe emodin had no effect on $AXIN2^+$ CBC number in organoids. This suggests that aloe emodin did not directly benefit CBC amplification, but increased LRCs that are eventually converted into additional CBCs. Our further results based on $SOX9^+$ region captured by LCM also supported that these aloe emodin-driven cells were $SOX9^+HOPX^+$ LRCs instead of $LGR5^+$ CBCs. It is worth noting that a previous study has identified a colitis-associated regenerative stem cell (CARSC) population that functionally contributes to mucosal repair in mouse colitis[53]. CARSCs are also marked by HOPX as well as LRCs, therefore CARSCs may differentiate from LRCs in colitis-associated regeneration. Considering that there is no evidence that CARSCs are precursor cells of EECs, we still use LRCs here to define these aloe emodin-driven cells. Recently, Hans Clever's group[54] used unbiased transcription factor CRISPR screen to identify a master repressor of EEC differentiation, and confirmed SOX4 as a direct target gene. Earlier studies have pointed out that the development of bile ducts is under precise control of the cooperative action of SOX4 and SOX9[55]. In conjunction with our study, this cooperation may dominate the EEC differentiation.

Evidence suggests that the intestinal epithelial cell-specific FOXO1 knockout disrupts mucin secretion and exacerbates inflammation in mice intestines, which is consistent with our results. We further linked nuclear translocation of FOXO1 to epithelial cell differentiation, creating a new therapeutic intervention point. Nuclear-activated FOXO1 controls the expression of downstream genes such as antioxidant stress enzymes, cell cycle arrest genes, and apoptosis-related genes[34]. Phosphorylation is a crucial post-translational modification of FOXO1, and AKT-mediated phosphorylation creates docking sites for the 14-3-3 proteins, which masks the nuclear localization signal, preventing FOXO1 from entering the nucleus[56,57]. Previous reports have indicated that FOXO1 is a negative regulator of $NEUROG3^+$ EEC differentiation[58-60]. FOXO1 deletion increases the number of the EEC population[59], and FOXO1 inhibition in EECs stimulates the conversion of EECs into insulin-producing cells[59,61]. One of these studies noted that this conversion is due to alterations in Notch (reduced *Hes1* expression) and Wnt signaling (increased *Aes* expression)[59], but did not give a more precise description at the molecular level. We do not believe that altered Wnt/Notch switch are the underlying causes. UMAP plots based single cell suggests that EECs have a particular transcriptional profile compared to other secretory epithelial cells. This indicates that EEC development might be controlled by different mechanisms than the Wnt/Notch switch that determines other secretory epithelial cell differentiation.

In our opinion, this is a sequential process, similar to pancreatic development, where NEUROG3 high expression in $SOX9^+$ cells causes cell-cycle exit and endocrine commitment[62]. In the intestine, high-turnover, high-stemness $SOX9^+$ LRCs progressively differentiate into distinctly functioning EECs, which requires FOXO1 inhibition. Persistent inhibition of FOXO1 promotes the differentiation of EEC into insulin-producing cells. Our data demonstrate at the molecular level that FOXO1 binds to the promoter region of SOX9, suggesting that FOXO1 controls this process through SOX9. For NEUROG3, there possibilities exist: (i) NEUROG3 might be an important controller of this process, and FOXO1 might be its transcriptional repressor; (ii) NEUROG3 might be an important controller of this process, but it is regulated by other transcription factors; (iii) NEUROG3 might just be a conspicuous marker, which undertakes certain functions but does not determine the direction of differentiation. All these need to be further investigated.

Moreover, it was observed, we found that several signaling pathways in clinical data including TGFβ, pyruvate metabolism, autophagy and nuclear factor kappa B (NF-κB) are associated with the balance of SOX9−NEUROG3 and have crosstalk with FOXO1 pathway. Insufficient TGFβ signaling is an important mechanism contributing to IBD pathogenesis[63,64], and TGFβ in

chondrocytes specifically regulates FOXO1 in a TGFβ activated kinase 1 (TAK1)-dependent manner[65]. The over-differentiation of LRC-EEC that we observed in CD patients and colitis mice might be due to the impaired TGFβ-FOXO1 pathway. Nuclear FOXO1 promotes the expression of pyruvate dehydrogenase kinase 4 (PDK4), which blocks pyruvate oxidative phosphorylation in mitochondria[66]. Consistently, Schell et al.[67] proposed that limiting mitochondrial pyruvate metabolism is necessary and sufficient to maintain the proliferation of CBCs. Interestingly, blocking mitochondrial oxidative phosphorylation results in Paneth cell abnormalities[4]. LRCs are also important precursors of Paneth cells in the small intestine, which suggests that enough oxidative phosphorylation may promote further differentiation of LRCs to EECs or Paneth cells, while impaired oxidative phosphorylation promotes LRCs to retain their current state or dedifferentiate into CBCs. However, considering that mature EECs themselves secrete glucagon-like peptide 1 (GLP1), which promotes oxidative phosphorylation[68], this may also be an adaptive regulation by mature EECs themselves. Furthermore, cytoplasmic, rather than nuclear, acetylated FOXO1 can interact with ATG7 thereby induce autophagy-induced cell death[69]. This implies that reducing cytoplasmic FOXO1 by aloe emodin may decrease cell death induced by excessive autophagy. NF-κB can shape metabolic adaptation by inhibiting FOXO-mediated lipolysis through the inhibition of histone deacetylation[70], suggesting that the inflammatory environment in colitis may contribute to the impaired FOXO1 function in epithelial cells, causing an to the imbalance of SOX9−NEUROG3. Certainly, considering that NF-κB activation is a typical feature of excessive inflammation, NF-κB enriching on opposing side just implies that FOXO1 activation would lead to comparatively lower levels of inflammation. We used the bromodomain-containing protein 4 (BRD4) specific inhibitor JQ-1 to inhibit SOX9 transcript levels when demonstrating the importance of SOX9 for aloe emodin. This result became interesting when we subsequently found that FOXO1 is a key transcription factor regulating SOX9. BRD4 acts as an epigenetic reader that binds to hyperacetylated chromatin regions, recruiting mediator complexes and chromatin modifiers to promote transcription initiation. JQ-1 represses SOX9 expression by blocking the binding of BRD4 to the DNA regulatory region of SOX9[32]. And, acetylation impairs (but does not completely block) the DNA-binding activity of FOXO1[71]. This raises the new possibility that BRD4 anchors the binding of acetylated FOXO1 to the SOX9 promoter sequence, which could be blocked by JQ-1.

FFAR1 is a GPCR that senses medium- to long-chain fatty acids. It is mainly expressed in pancreatic beta cells and enteroendocrine cells, where it mediates glucose-dependent insulin secretion and sensitivity. The FFAR1-activated Gαq signaling triggers the release of Ca^{2+} into the cytoplasm, activation of protein kinase C, and enhancement of insulin and enteric proinsulin hormone release. Therefore, compounds targeting FFAR1 can be effective treatments for type 2 diabetes[72]. Although the exact functions of FFAR1 within the gut are still being explored, our study reveals a novel mechanism. We discovered that activating FFAR1 directly sets off a signaling cascade involving PI3K/AKT/p-FOXO1. This process is mediated by the Gβ2γ3 subunit and ultimately leads to the differentiation of EECs that produce the hormone glucagon (GCG). Furthermore, we identified a plant-derived FFAR1 antagonist. Studies have shown that PI3K/AKT activation inhibits FOXO1, but it is generally believed that its activation occurs through insulin-stimulated insulin receptor (IR) tyrosine kinase rather than GPCR activation[73]. Our data revealed that activated FFAR1 promotes AKT phosphorylation at the Thr308 site through G$\beta\gamma$, thereby phosphorylating FOXO1 and sequestering it in the cytoplasm. Furthermore, we observed a preference for Gβ2 when FFAR1 was activated. When considering previous research[41], Gβ2Gγ3 may be the predominant combination for GPCR-mediated AKT phosphorylation signaling. Consistent with our results, linoleic acid, an endogenous ligand of FFAR1, has recently been reported to increase susceptibility to IBD[74-76], while previous views would suggest that this involves an altered metabolic phenotype of inflammatory cells. Here we provide a description of how linoleic acid metabolism alters epithelial cell differentiation, potentially expanding knowledge of the impact of dietary structure on intestinal disease. Furthermore, FFAR1 is also expressed on immune cells like neutrophils and macrophages, where it contributes to the regulation of the immune response mediated by medium- and long-chain fatty acids. FFAR1 activation in neutrophils enhances IL-8 expression and chemotaxis and prolongs neutrophil lifespan[77-80], leading to pro-inflammatory phenotype. In contrast, in macrophages, FFAR1 agonists induced macrophage anti-inflammatory phenotype by mechanisms that may be related to the expression of ATP-binding cassette (ABC) transporter proteins[81] or nuclear localization of NF-κB[82,83]. Theoretically, aloe emodin treatment tmay decrease the FFAR1 activity in both neutrophils and macrophages, leading to a mixed effect on the inflammatory phenotype. Our results showed that aloe emodin as an FFAR1 inhibitor alleviated inflammation in the DSS model, suggesting that aloe emodin-mediated anti-inflammatory effects on neutrophils and epithelial cells outweighed its pro-inflammatory effects on macrophage cells. This may be explained by the different abundance of FFAR1 expression (FFAR1 expression on enteroendocrine cells was significantly higher than on other cells in gut[84]), and the different degree of exposure to the drug (neutrophil and epithelial cells are physically closer to the intestinal lumen in colitis[85]).

5. Conclusions

In conclusion, our study demonstrates that an anthraquinone analogue from a traditional medicinal plant can suppress the over-differentiation of EECs caused by activation of long-chain fatty acid receptor FFAR1 in colitis, potentially providing new insights into the treatment of IBD.

Acknowledgments

This study was supported by National Natural Science Foundation of China (Nos. 82030113, 82130108, and 82204717) and China Postdoctoral Science Foundation (Nos. BX20220069 and 2021M700864).

Author contributions

Weilian Bao: Data curation, Formal analysis, Funding acquisition, Investigation, Methodology, Project administration, Software, Visualization, Writing − original draft. Jiaren Lyu: Data curation, Formal analysis, Investigation, Methodology, Software, Validation, Visualization. Guize Feng: Data curation, Formal analysis, Investigation, Methodology, Visualization, Writing − original draft. Linfeng Guo: Validation. Dian Zha: Investigation. Keyuan You: Investigation. Yang Liu: Methodology, Software. Haidong Li: Methodology. Peng Du: Resources, Supervision. Daofeng

Chen: Conceptualization, Funding acquisition, Project administration, Resources, Supervision, Writing − review & editing. Xiaoyan Shen: Conceptualization, Funding acquisition, Project administration, Resources, Supervision, Writing − review & editing.

Conflicts of interest

The authors declare no conflicts of interest.

Appendix A. Supporting information

Supporting information to this article can be found online at https://doi.org/10.1016/j.apsb.2024.05.027.

References

1. Villablanca EJ, Selin K, Hedin CRH. Mechanisms of mucosal healing: treating inflammatory bowel disease without immunosuppression? *Nat Rev Gastroenterol Hepatol* 2022;**19**:493−507.
2. Neurath MF, Travis SP. Mucosal healing in inflammatory bowel diseases: a systematic review. *Gut* 2012;**61**:1619−35.
3. Beumer J, Clevers H. Cell fate specification and differentiation in the adult mammalian intestine. *Nat Rev Mol Cell Biol* 2021;**22**:39−53.
4. Khaloian S, Rath E, Hammoudi N, Gleisinger E, Blutke A, Giesbertz P, et al. Mitochondrial impairment drives intestinal stem cell transition into dysfunctional Paneth cells predicting Crohn's disease recurrence. *Gut* 2020;**69**:1939−51.
5. Elmentaite R, Ross ADB, Roberts K, James KR, Ortmann D, Gomes T, et al. Single-cell sequencing of developing human gut reveals transcriptional links to childhood Crohn's disease. *Dev Cell* 2020;**55**:771−83.
6. Suzuki K, Murano T, Shimizu H, Ito G, Nakata T, Fujii S, et al. Single cell analysis of Crohn's disease patient-derived small intestinal organoids reveals disease activity-dependent modification of stem cell properties. *J Gastroenterol* 2018;**53**:1035−47.
7. Kanke M, Kennedy Ng MM, Connelly S, Singh M, Schaner M, Shanahan MT, et al. Single-cell analysis reveals unexpected cellular changes and transposon expression signatures in the colonic epithelium of treatment-naive adult Crohn's disease patients. *Cell Mol Gastroenterol Hepatol* 2022;**13**:1717−40.
8. Ayyaz A, Kumar S, Sangiorgi B, Ghoshal B, Gosio J, Ouladan S, et al. Single-cell transcriptomes of the regenerating intestine reveal a revival stem cell. *Nature* 2019;**569**:121−5.
9. Roche KC, Gracz AD, Liu XF, Newton V, Akiyama H, Magness ST. SOX9 maintains reserve stem cells and preserves radioresistance in mouse small intestine. *Gastroenterology* 2015;**149**:1553−63.
10. Buczacki SJ, Zecchini HI, Nicholson AM, Russell R, Vermeulen L, Kemp R, et al. Intestinal label-retaining cells are secretory precursors expressing Lgr5. *Nature* 2013;**495**:65−9.
11. El-Salhy M, Danielsson A, Stenling R, Grimelius L. Colonic endocrine cells in inflammatory bowel disease. *J Intern Med* 1997;**242**:413−9.
12. Worthington JJ, Reimann F, Gribble FM. Enteroendocrine cells-sensory sentinels of the intestinal environment and orchestrators of mucosal immunity. *Mucosal Immunol* 2018;**11**:3−20.
13. Kidd M, Gustafsson BI, Drozdov I, Modlin IM. IL1β- and LPS-induced serotonin secretion is increased in EC cells derived from Crohn's disease. *Neurogastroenterol Motil* 2009;**21**:439−50.
14. Eissa N, Hussein H, Kermarrec L, Elgazzar O, Metz-Boutigue MH, Bernstein CN, et al. Chromofungin (CHR: CHGA(47-66)) is down-regulated in persons with active ulcerative colitis and suppresses pro-inflammatory macrophage function through the inhibition of NF-κB signaling. *Biochem Pharmacol* 2017;**145**:102−13.
15. Cao YJ, Pu ZJ, Tang YP, Shen J, Chen YY, Kang A, et al. Advances in bio-active constituents, pharmacology and clinical applications of rhubarb. *Chin Med* 2017;**12**:36.
16. Dong X, Zeng Y, Liu Y, You L, Yin X, Fu J, et al. Aloe-emodin: a review of its pharmacology, toxicity, and pharmacokinetics. *Phytother Res* 2020;**34**:270−81.
17. Sato T, Stange DE, Ferrante M, Vries RG, Van Es JH, Van den Brink S, et al. Long-term expansion of epithelial organoids from human colon, adenoma, adenocarcinoma, and Barrett's epithelium. *Gastroenterology* 2011;**141**:1762−72.
18. Rodriguez-Colman MJ, Schewe M, Meerlo M, Stigter E, Gerrits J, Pras-Raves M, et al. Interplay between metabolic identities in the intestinal crypt supports stem cell function. *Nature* 2017;**543**:424−7.
19. Wirtz S, Popp V, Kindermann M, Gerlach K, Weigmann B, Fichtner-Feigl S, et al. Chemically induced mouse models of acute and chronic intestinal inflammation. *Nat Protoc* 2017;**12**:1295−309.
20. Okayasu I, Hatakeyama S, Yamada M, Ohkusa T, Inagaki Y, Nakaya R. A novel method in the induction of reliable experimental acute and chronic ulcerative colitis in mice. *Gastroenterology* 1990;**98**:694−702.
21. Chen G, Ran X, Li B, Li Y, He D, Huang B, et al. Sodium butyrate inhibits inflammation and maintains epithelium barrier integrity in a TNBS-induced inflammatory bowel disease mice model. *EBioMedicine* 2018;**30**:317−25.
22. Weigmann B, Tubbe I, Seidel D, Nicolaev A, Becker C, Neurath MF. Isolation and subsequent analysis of murine lamina propria mononuclear cells from colonic tissue. *Nat Protoc* 2007;**2**:2307−11.
23. Wroblewska A, Dhainaut M, Ben-Zvi B, Rose SA, Park ES, Amir ED, et al. Protein barcodes enable high-dimensional single-cell CRISPR screens. *Cell* 2018;**175**:1141−55.
24. Chen Z, Arai E, Khan O, Zhang Z, Ngiow SF, He Y, et al. *In vivo* $CD8^+$ T cell CRISPR screening reveals control by Fli1 in infection and cancer. *Cell* 2021;**184**:1262−80.
25. Gu W, Colarusso JL, Dame MK, Spence JR, Zhou Q. Rapid establishment of human colonic organoid knockout lines. *STAR Protoc* 2022;**3**:101308.
26. Parikh K, Antanaviciute A, Fawkner-Corbett D, Jagielowicz M, Aulicino A, Lagerholm C, et al. Colonic epithelial cell diversity in health and inflammatory bowel disease. *Nature* 2019;**567**:49−55.
27. Peters LA, Perrigoue J, Mortha A, Iuga A, Song WM, Neiman EM, et al. A functional genomics predictive network model identifies regulators of inflammatory bowel disease. *Nat Genet* 2017;**49**:1437−49.
28. Fu S, Zhou Y, Hu C, Xu Z, Hou J. Network pharmacology and molecular docking technology-based predictive study of the active ingredients and potential targets of rhubarb for the treatment of diabetic nephropathy. *BMC Complement Med Ther* 2022;**22**:210.
29. Zhang WW, Yao CL, Chen XB, Wei XM, Chen L, Zhnag JQ, et al. Identification of chemical constituents of Xiaochengqi Decoction by UPLC−Q-TOF/Fast DDA combined with UNIFI software. *Zhongguo Zhong Yao Za Zhi* 2022;**47**:2121−33.
30. Gehart H, van Es JH, Hamer K, Beumer J, Kretzschmar K, Dekkers JF, et al. Identification of enteroendocrine regulators by real-time single-cell differentiation mapping. *Cell* 2019;**176**:1158−73.
31. Grabinger T, Luks L, Kostadinova F, Zimberlin C, Medema JP, Leist M, et al. *Ex vivo* culture of intestinal crypt organoids as a model system for assessing cell death induction in intestinal epithelial cells and enteropathy. *Cell Death Dis* 2014;**5**:e1228.
32. Hong SH, You JS. SOX9 is controlled by the BRD4 inhibitor JQ1 *via* multiple regulation mechanisms. *Biochem Biophys Res Commun* 2019;**511**:746−52.
33. Eijkelenboom A, Burgering BM. FOXOs: signalling integrators for homeostasis maintenance. *Nat Rev Mol Cell Biol* 2013;**14**:83−97.
34. Calissi G, Lam EW, Link W. Therapeutic strategies targeting FOXO transcription factors. *Nat Rev Drug Discov* 2021;**20**:21−38.
35. Brunet A, Bonni A, Zigmond MJ, Lin MZ, Juo P, Hu LS, et al. Akt promotes cell survival by phosphorylating and inhibiting a Forkhead transcription factor. *Cell* 1999;**96**:857−68.
36. Cahill CM, Tzivion G, Nasrin N, Ogg S, Dore J, Ruvkun G, et al. Phosphatidylinositol 3-kinase signaling inhibits DAF-16 DNA binding and function *via* 14-3-3-dependent and 14-3-3-independent pathways. *J Biol Chem* 2001;**276**:13402−10.

37. Itoh Y, Kawamata Y, Harada M, Kobayashi M, Fujii R, Fukusumi S, et al. Free fatty acids regulate insulin secretion from pancreatic beta cells through GPR40. *Nature* 2003;**422**:173−6.
38. Tsujihata Y, Ito R, Suzuki M, Harada A, Negoro N, Yasuma T, et al. TAK-875, an orally available G protein-coupled receptor 40/free fatty acid receptor 1 agonist, enhances glucose-dependent insulin secretion and improves both postprandial and fasting hyperglycemia in type 2 diabetic rats. *J Pharmacol Exp Ther* 2011;**339**:228−37.
39. Dbouk HA, Vadas O, Shymanets A, Burke JE, Salamon RS, Khalil BD, et al. G protein-coupled receptor-mediated activation of p110beta by G$\beta\gamma$ is required for cellular transformation and invasiveness. *Sci Signal* 2012;**5**:ra89.
40. Vadas O, Dbouk HA, Shymanets A, Perisic O, Burke JE, Abi Saab WF, et al. Molecular determinants of PI3Kγ-mediated activation downstream of G-protein-coupled receptors (GPCRs). *Proc Natl Acad Sci U S A* 2013;**110**:18862−7.
41. Wijayaratna D, Ratnayake K, Ubeysinghe S, Kankanamge D, Tennakoon M, Karunarathne A. The spatial distribution of GPCR and G$\beta\gamma$ activity across a cell dictates PIP3 dynamics. *Sci Rep* 2023;**13**:2771.
42. Rees WD, Tandun R, Yau E, Zachos NC, Steiner TS. Regenerative intestinal stem cells induced by acute and chronic injury: the saving grace of the epithelium? *Front Cell Dev Biol* 2020;**8**:583919.
43. Graham WV, He W, Marchiando AM, Zha J, Singh G, Li HS, et al. Intracellular MLCK1 diversion reverses barrier loss to restore mucosal homeostasis. *Nat Med* 2019;**25**:690−700.
44. Bai D, Zhao J, Wang R, Du J, Zhou C, Gu C, et al. *Eubacterium coprostanoligenes* alleviates chemotherapy-induced intestinal mucositis by enhancing intestinal mucus barrier. *Acta Pharm Sin B* 2024;**14**:1677−92.
45. Li H, Zhang Y, Liu MT, Fan C, Feng CL, Lu QK, et al. Targeting PDE4 as a promising therapeutic strategy in chronic ulcerative colitis through modulating mucosal homeostasis. *Acta Pharm Sin B* 2022;**12**:228−45.
46. Gomollon F, Dignass A, Annese V, Tilg H, Van Assche G, Lindsay JO, et al. 3rd European evidence-based consensus on the diagnosis and management of Crohn's disease 2016: part 1: diagnosis and medical management. *J Crohns Colitis* 2017;**11**:3−25.
47. Harbord M, Eliakim R, Bettenworth D, Karmiris K, Katsanos K, Kopylov U, et al. Third European evidence-based consensus on diagnosis and management of ulcerative colitis. Part 2: current management. *J Crohns Colitis* 2017;**11**:769−84.
48. Rutgeerts P, Van Assche G, Sandborn WJ, Wolf DC, Geboes K, Colombel JF, et al. Adalimumab induces and maintains mucosal healing in patients with Crohn's disease: data from the EXTEND trial. *Gastroenterology* 2012;**142**:1102−11.e2.
49. Hu B, Zhang H, Meng X, Wang F, Wang P. Aloe-emodin from rhubarb (Rheum rhabarbarum) inhibits lipopolysaccharide-induced inflammatory responses in RAW264.7 macrophages. *J Ethnopharmacol* 2014;**153**:846−53.
50. Bao W, You Y, Ni J, Hou H, Lyu J, Feng G, et al. Inhibiting sorting nexin 10 promotes mucosal healing through SREBP2-mediated stemness restoration of intestinal stem cells. *Sci Adv* 2023;**9**:eadh5016.
51. Kubota A, Terasaki M, Takai R, Kobayashi M, Muromoto R, Kojima H. 5-Aminosalicylic acid, a weak agonist for aryl hydrocarbon receptor that induces splenic regulatory T cells. *Pharmacology* 2022;**107**:28−34.
52. Oh-Oka K, Kojima Y, Uchida K, Yoda K, Ishimaru K, Nakajima S, et al. Induction of colonic regulatory T cells by mesalamine by activating the Aryl hydrocarbon receptor. *Cell Mol Gastroenterol Hepatol* 2017;**4**:135−51.
53. Wang Y, Chiang IL, Ohara TE, Fujii S, Cheng J, Muegge BD, et al. Long-term culture captures injury-repair cycles of colonic stem cells. *Cell* 2019;**179**:1144−59.
54. Lin L, DeMartino J, Wang D, van Son GJF, van der Linden R, Begthel H, et al. Unbiased transcription factor CRISPR screen identifies ZNF800 as master repressor of enteroendocrine differentiation. *Science* 2023;**382**:451−8.
55. Poncy A, Antoniou A, Cordi S, Pierreux CE, Jacquemin P, Lemaigre FP. Transcription factors SOX4 and SOX9 cooperatively control development of bile ducts. *Dev Biol* 2015;**404**:136−48.
56. Brunet A, Kanai F, Stehn J, Xu J, Sarbassova D, Frangioni JV, et al. 14-3-3 transits to the nucleus and participates in dynamic nucleocytoplasmic transport. *J Cell Biol* 2002;**156**:817−28.
57. Su YW, Hao Z, Hirao A, Yamamoto K, Lin WJ, Young A, et al. 14-3-3sigma regulates B-cell homeostasis through stabilization of FOXO1. *Proc Natl Acad Sci U S A* 2011;**108**:1555−60.
58. McKimpson WM, Kuo T, Kitamoto T, Higuchi S, Mills JC, Haeusler RA, et al. FOXO1 is present in stomach epithelium and determines gastric cell distribution. *Gastro Hep Adv* 2022;**1**:733−45.
59. Talchai C, Xuan S, Kitamura T, DePinho RA, Accili D. Generation of functional insulin-producing cells in the gut by Foxo1 ablation. *Nat Genet* 2012;**44**:406−12.
60. Ludikhuize MC, Meerlo M, Gallego MP, Xanthakis D, Burgaya Julia M, Nguyen NTB, et al. Mitochondria define intestinal stem cell differentiation downstream of a FOXO/Notch axis. *Cell Metab* 2020;**32**:889−900.e7.
61. Bouchi R, Foo KS, Hua H, Tsuchiya K, Ohmura Y, Sandoval PR, et al. FOXO1 inhibition yields functional insulin-producing cells in human gut organoid cultures. *Nat Commun* 2014;**5**:4242.
62. Bechard ME, Bankaitis ED, Ustione A, Piston DW, Magnuson MA, Wright CVE. FUCCI tracking shows cell-cycle-dependent Neurog3 variation in pancreatic progenitors. *Genesis* 2017;**55**. DOI:10.1002/dvg.23050.
63. Ihara S, Hirata Y, Koike K. TGF-β in inflammatory bowel disease: a key regulator of immune cells, epithelium, and the intestinal microbiota. *J Gastroenterol* 2017;**52**:777−87.
64. Monteleone G, Boirivant M, Pallone F, MacDonald TT. TGF-β1 and Smad7 in the regulation of IBD. *Mucosal Immunol* 2008;**1**(Suppl. 1):S50−3.
65. Wang C, Shen J, Ying J, Xiao D, O'Keefe RJ. FoxO1 is a crucial mediator of TGF-β/TAK1 signaling and protects against osteoarthritis by maintaining articular cartilage homeostasis. *Proc Natl Acad Sci U S A* 2020;**117**:30488−97.
66. Gopal K, Saleme B, Al Batran R, Aburasayn H, Eshreif A, Ho KL, et al. FoxO1 regulates myocardial glucose oxidation rates *via* transcriptional control of pyruvate dehydrogenase kinase 4 expression. *Am J Physiol Heart Circ Physiol* 2017;**313**:H479−90.
67. Schell JC, Wisidagama DR, Bensard C, Zhao H, Wei P, Tanner J, et al. Control of intestinal stem cell function and proliferation by mitochondrial pyruvate metabolism. *Nat Cell Biol* 2017;**19**:1027−36.
68. Carlessi R, Chen Y, Rowlands J, Cruzat VF, Keane KN, Egan L, et al. GLP-1 receptor signalling promotes β-cell glucose metabolism *via* mTOR-dependent HIF-1α activation. *Sci Rep* 2017;**7**:2661.
69. Zhao Y, Yang J, Liao W, Liu X, Zhang H, Wang S, et al. Cytosolic FoxO1 is essential for the induction of autophagy and tumour suppressor activity. *Nat Cell Biol* 2010;**12**:665−75.
70. Molaei M, Vandehoef C, Karpac J. NF-κB shapes metabolic adaptation by attenuating Foxo-mediated lipolysis in *Drosophila*. *Dev Cell* 2019;**49**:802−810.e6.
71. Matsuzaki H, Daitoku H, Hatta M, Aoyama H, Yoshimochi K, Fukamizu A. Acetylation of Foxo1 alters its DNA-binding ability and sensitivity to phosphorylation. *Proc Natl Acad Sci U S A* 2005;**102**:11278−83.
72. Li Z, Zhou Z, Zhang L. Current status of GPR40/FFAR1 modulators in medicinal chemistry (2016−2019): a patent review. *Expert Opin Ther Pat* 2020;**30**:27−38.
73. Ni YG, Wang N, Cao DJ, Sachan N, Morris DJ, Gerard RD, et al. FoxO transcription factors activate Akt and attenuate insulin signaling in heart by inhibiting protein phosphatases. *Proc Natl Acad Sci U S A* 2007;**104**:20517−22.
74. Deol P, Ruegger P, Logan GD, Shawki A, Li J, Mitchell JD, et al. Diet high in linoleic acid dysregulates the intestinal endocannabinoid system and increases susceptibility to colitis in mice. *Gut Microbes* 2023;**15**:2229945.

75. Jia X, Hu C, Wu X, Qi H, Lin L, Xu M, et al. Evaluating the effects of omega-3 polyunsaturated fatty acids on inflammatory bowel disease *via* circulating metabolites: a mediation mendelian randomization study. *Metabolites* 2023;**13**:1041.
76. Yu T, Zhou Z, Liu S, Li C, Zhang ZW, Zhang Y, et al. The role of phosphatidylcholine 34:1 in the occurrence, development and treatment of ulcerative colitis. *Acta Pharm Sin B* 2023;**13**:1231−45.
77. Hidalgo MA, Nahuelpan C, Manosalva C, Jara E, Carretta MD, Conejeros I, et al. Oleic acid induces intracellular calcium mobilization, MAPK phosphorylation, superoxide production and granule release in bovine neutrophils. *Biochem Biophys Res Commun* 2011;**409**:280−6.
78. Manosalva C, Mena J, Velasquez Z, Colenso CK, Brauchi S, Burgos RA, et al. Cloning, identification and functional characterization of bovine free fatty acid receptor-1 (FFAR1/GPR40) in neutrophils. *PLoS One* 2015;**10**:e0119715.
79. Mena SJ, Manosalva C, Carretta MD, Teuber S, Olmo I, Burgos RA, et al. Differential free fatty acid receptor-1 (FFAR1/GPR40) signalling is associated with gene expression or gelatinase granule release in bovine neutrophils. *Innate Immun* 2016;**22**:479−89.
80. Souza PR, Walker ME, Goulding NJ, Dalli J, Perretti M, Norling LV. The GPR40 agonist GW9508 enhances neutrophil function to aid bacterial clearance during *E. coli* infections. *Front Immunol* 2020;**11**:573019.
81. An T, Zhang X, Li H, Dou L, Huang X, Man Y, et al. GPR120 facilitates cholesterol efflux in macrophages through activation of AMPK signaling pathway. *FEBS J* 2020;**287**:5080−95.
82. Kim JW, Roh E, Choi KM, Yoo HJ, Hwang HJ, Baik SH. GPR40 agonism modulates inflammatory reactions in vascular endothelial cells. *Diabetes Metab J* 2022;**46**:506−11.
83. Zhao T, Zhou Z, Zhao S, Wan H, Li H, Hou J, et al. Vincamine as an agonist of G protein-coupled receptor 40 effectively ameliorates pulmonary fibrosis in mice. *Phytomedicine* 2023;**118**:154919.
84. Petersen JE, Pedersen MH, Dmytriyeva O, Nellemose E, Arora T, Engelstoft MS, et al. Free fatty acid receptor 1 stimulates cAMP production and gut hormone secretion through Gq-mediated activation of adenylate cyclase 2. *Mol Metab* 2023;**74**:101757.
85. Garrido-Trigo A, Corraliza AM, Veny M, Dotti I, Melon-Ardanaz E, Rill A, et al. Macrophage and neutrophil heterogeneity at single-cell spatial resolution in human inflammatory bowel disease. *Nat Commun* 2023;**14**:4506.